WAVE PROPAGATION IN PRESTRAINED POLYETHYLENE RODS

Thesis for the Degree of Ph. D.

MICHIGAN STATE UNIVERSITY

ALDRED L. STEVENS

1968

This is to certify that the

thesis entitled

WAVE PROPAGATION IN PRESTRAINED

POLYETHYLENE RODS

presented by

Aldred L. Stevens

has been accepted towards fulfillment
of the requirements for

Ph. D. degree in Mechanics

Lawrence E. Malvern
Major professor

Date March 11, 1968

O-169

ABSTRACT

WAVE PROPAGATION IN PRESTRAINED
POLYETHYLENE RODS

by Aldred L. Stevens

The influence of prestrain on the propagation of mechanical waves along a slender rod of low-density unoriented polyethylene was experimentally investigated. The investigation consisted of two major parts: first, a uniaxial continuous-wave technique was used to determine the dynamic mechanical properties of the polyethylene in the form of the frequency-dependent phase velocity and damping factor for frequencies spanning the audio spectrum and for levels of uniaxial static prestrain up to 10%. A linear incremental dynamic viscoelastic behavior about a state of finite static prestrain was shown to obtain over the range of strains and frequencies used.

In the second part, the propagation of an incremental strain pulse along a slender rod of the same material used in the first part was investigated. With the rod in a state of static prestrain, an incremental impact-induced strain pulse was introduced into the polyethylene rod and monitored at two positions along the rod. Assuming

a linear incremental dynamic viscoelastic behavior of the material, the equations necessary to describe the resulting uniaxial strain as a function of time and position along the rod are presented and the solution obtained by Fourier transform methods. The resulting Fourier inverse transform was numerically evaluated, using the material properties determined in the first part. The strain measured at the first position was used as the input boundary condition for computing the strain at the second position.

Results of the continuous-wave studies indicate that the phase velocity decreases and the damping factor increases with increasing prestrain in the range of prestrains. For example, at 8% prestrain the decrease in phase velocity is approximately 4% and the increase in the damping factor is approximately 25%. The change in the phase velocity with prestrain is relatively uniform over the audio-frequency range.

Good correlation of the leading edges of the experimentally measured and numerically synthesized strain pulses supports the high-frequency phase velocity data of the first part. Discrepancies between the measured and synthesized pulse shapes were noted which are believed to be associated with the problem of measuring strain in low modulus materials with conventional strain gages.

WAVE PROPAGATION IN PRESTRAINED POLYETHYLENE RODS

By

yman
Aldred L. Stevens

A THESIS

Submitted to
Michigan State University
in partial fulfillment of the requirements
for the degree of

DOCTOR OF PHILOSOPHY

Department of Metallurgy, Mechanics and
Materials Science

1968

G 5/535
10/8/68

ACKNOWLEDGMENTS

To the many people who have helped and encouraged me; especially to Dr. L. E. Malvern for his generous contribution of time and valuable counsel throughout the study, and to the members of my guidance committee, Dr. G. E. Mase, Dr. T. Triffet and Dr. P. K. Wong, I offer my most grateful thanks.

This work was supported by the National Science Foundation under Grant Number G1369X. The first two years of advanced graduate study were made possible by a National Science Foundation Cooperative Graduate Fellowship.

TABLE OF CONTENTS

Page

LIST OF TABLES

LIST OF FIGURES

Figure		Page

I. INTRODUCTION

1.1. Purpose of Investigation and Brief Statement of Results

The general objective of this research was to determine the influence of various moderate amounts (less than 10%) of quasistatic prestrain upon the dynamic response of low-density polyethylene when small increments of dynamic strain were superposed on the prestrain.

The experimental investigation consisted of two major parts: (1) sinusoidal continuous-wave propagation studies to determine the incremental phase velocity and damping, and (2) impact-induced pulse propagation studies. In the first part the dynamic mechanical properties of low-density polyethylene in the form of a slender rod were determined as a function of the frequency and the prestrain. In this continuous-wave study the prestrain was the constant mean strain upon which the sinusoidal incremental strain was superposed. In the second experimental study longitudinal tensile impacts induced transient incremental strain pulses, which propagated along rods of the same material and same size as those used in the continuous-wave studies, at the same levels of prestrain.

Although the response of the material to dynamic strains of the order of 10% is nonlinear, the incremental dynamic response for small incremental waves superposed on prestrains up to 10% was assumed to be linear, which was verified in the continuous-wave studies for various incremental strain amplitudes up to 400 microinches per inch.

The impact-induced pulse propagation was then analyzed, assuming a linear incremental response superposed on the prestrain, by Fourier analysis and synthesis, using the properties determined in the continuous-wave studies. The results predicted by the Fourier synthesis are compared with the pulse-propagation experimental results in Section 3.4.

Previous investigations of the effect of prestrain upon the dynamic mechanical properties are limited. Hillier and Kolsky [1]* have studied the propagation of single-frequency continuous waves along filaments of several polymers while the filaments were being stretched at a constant rate. Mason [2] and Hillier [3] have studied the influence of strain upon the dynamic mechanical properties of natural rubber. Both investigations were primarily concerned with large prestrains, up to 600% elongation.

---

*Numbers in brackets refer to the list of references at the end of the paper.

Hillier and Kolsky indicated that, for a fixed strain, the change in the dynamic modulus during the relaxation of stress was "extremely small." The present investigator was thus influenced to study the dependence of the dynamic mechanical properties upon prestrain, as opposed to dependence upon prestress.

The results of the present investigations indicate that, for prestrains up to approximately 10%, the phase velocity c decreases with increasing prestrain and the damping factor α increases with increasing prestrain, over the complete audio frequency range used in this investigation. This result was qualitatively supported by the correlation between the measured pulse traveling along the polyethylene rod and the predicted pulse as synthesized by Fourier techniques using the dynamic mechanical properties previously determined.

The effect of moderate prestrain on the dynamic properties may have practical importance because the mechanical failure of polymer structural elements in many realistic situations involves the dynamic loading of the material while it is in a strained state. For example, the viscoelastic solid fuel in a rocket is exposed during the firing sequence to an essentially quasistatic deformation, due to the acceleration forces, upon which is superposed the high-frequency deformations due to turbulent loads and vibrations. As another example, during the growth of a crack in tensile failure the polymer may be subjected to dynamic loads in addition to the quasistatic extensions in the area of the crack. In view of the effects of elongation upon the dynamic behavior of polymers, as discussed below, it is evident that the use of dynamic properties measured at essentially zero prestrain could be misleading.

To place in perspective the problem to which the investigation is addressed, a brief history of the development of the theory of viscoelasticity is given in the following section with attention focused mainly upon the dynamic properties of polymers. Then previous experimental work leading to this investigation is discussed in some detail in Section 1.3.

Part II is concerned with the investigation to achieve the first major objective of this research, the determination of the dynamic mechanical properties of polyethylene as a function of frequency and prestrain. In Part III the propagation of a longitudinal strain pulse in a prestrained polyethylene rod is investigated, the second major area of this work. The experimental results are compared in Section 3.4 with the analysis by Fourier transform methods based on the mechanical properties determined in Part II. A summary of results and conclusions and comments on continuing research in this area are presented in Part IV.

1.2. Historical Background

The phenomenological theory of viscoelasticity dates from the nineteenth century. In 1835 Weber [4] described the "elastic after-effect" in silk fibers and developed an empirical expression relating elongation to time under constant load. Boltzmann [5] gave the first mathematical statement of linear viscoelasticity, the now well-known superposition principle. However, the application of the theory of viscoelasticity has lagged far behind in comparison to the field of elasticity, where active research has been pursued for more than a century.

In the last twenty-five years there has been an increased interest in the mechanics of viscoelastic materials and structures. The introduction and rapid increase in the use of polymers as structural materials has provided a practical stimulus for the development of the mathematical theory of viscoelasticity.

From the standpoint of engineering analysis, the essential difference between viscoelastic materials and elastic materials is the rate and temperature dependence in the constitutive equation, the relation between stress and strain. This complexity in the constitutive equation is one reason for the delay in the development of applications of the formal theory of viscoelasticity.

A considerable development has been made for linearly viscoelastic materials, or materials assumed to be linear for a limited range of strain. Linear viscoelasticity implies that, at any instant, the magnitude of a time-dependent response is directly proportional to the magnitude of the applied time-dependent input. This assumption has proved to be sufficiently precise for many applications of polymer materials.

The mathematical aspects of linear viscoelasticity were greatly simplified by the integral transform techniques introduced by Gross [6]. Several papers [7, 8, 9] have been published giving useful approximate methods for interconverting expressions for the various mechanical properties of linear viscoelastic materials. Three distinct forms of the constitutive equations have been developed for describing the mechanical behavior of viscoelastic materials. They are the

1. Differential-operator (operational modulus) form;
2. Integral-operator (hereditary integral) form;
3. Complex modulus and compliance.

These are mathematically equivalent descriptions and can be interconverted by the transform techniques presented by Gross.

The differential-operator form was developed essentially in conjunction with the mechanical "spring-dashpot" models. The models provide insight into the phenomenological behavior of viscoelastic materials, but are not essential to the theory. A realistic description of most viscoelastic materials requires many-element models and consequent high-order ($\sim$10) differential constitutive equations. The resulting difficulties associated with initial and boundary conditions and the numerical solution of systems of high-order differential equations have diminished the practical use of this form. The integral-operator form is most conveniently used in quasistatic analyses where creep and/or relaxation functions are available for the material. Both of these forms have been used primarily in the area of quasistatic structural analysis or stress analysis. Excellent reviews of the development and use of these forms may be found in books by Leaderman [10], Alfrey [11], Gross [6], Bland [12], Ferry [13], and Flügge [14], and papers by Lee [15], Williams [16], and Ward and Pinnock [17].

Laplace-transform techniques may be applied to great advantage with these two forms of the constitutive equation used in quasistatic stress analysis. By using integral transforms, a system of differential or integral equations can be replaced by much simpler algebraic relations. The Laplace-transform of the constitutive equation has the effect of displaying the time dependence of the material in terms of a spectrum of time (decay) constants as expressed by the transform parameter. Schapery [18, 19] has presented two methods of fitting experimentally determined creep and stress-relaxation functions by a Dirichlet (or Prony) series, a "Fourier series" expansion in terms of real exponentials, of an arbitrary number of terms. The Laplace-transform of this series is well known. The solution of the resulting system of equations in transform space can be inverted by approximate techniques presented in recent papers by Arenz [20, 21] and Cost [22].

Since the primary concern of this paper is that of dynamic mechanical properties, further comments will be restricted to the third form of the constitutive equation, the complex modulus and compliance.

If a linearly-viscoelastic specimen is subjected to an alternating uniaxial stress, $\sigma = \sigma_0 e^{i\omega t}$, varying sinusoidally with circular frequency ω, the resulting uniaxial strain will be $\varepsilon = \varepsilon_0 e^{i(\omega t - \delta)}$. Then, in analogy to an elastic system, the relationship between uniaxial stress and uniaxial strain can be defined by a frequency dependent complex modulus $E(i\omega)$ as follows:

$$E(i\omega) = \frac{\sigma}{\varepsilon} = \frac{\sigma_0}{\varepsilon_0} e^{i\delta} = E^* e^{i\delta} = E_1 + iE_2 \qquad (1.2\text{-}1)$$

The behavior of the material in this type of loading can be completely described by a pair of quantities: the in-phase component E_1 and the 90°-out-of-phase component E_2 of the complex ratio of stress to strain, or equivalently, the phase angle δ and the ratio $\sigma_o/\varepsilon_o = E^*$. Still another equivalent pair, the phase velocity c and damping factor α are defined in Section 2.2. The frequency-dependent parameter $E^* = E(i\omega)$ is often simply called the modulus; E_1 is the storage modulus and E_2 is the loss modulus. A complex compliance $J(i\omega) = 1/E(i\omega)$ can be similarly defined.

In the complex-modulus representation the mechanical behavior of a linearly-viscoelastic material at a given temperature can be completely defined by the laboratory measurement of the two components of the complex modulus, or any of the equivalent pairs, as a function of frequency. This representation is most important when experimental work is to be correlated with theoretical analyses of transient pulse propagation. Fourier-transform methods are regularly used to transform the field equations and the initial and boundary conditions onto the frequency plane. The system of transformed equations is solved in transformed space in conjunction with the frequency-dependent material properties. Inversion back to the time domain is then accomplished either in closed form or, more generally, by numerical techniques. An excellent review of the theory of Fourier transform methods and associated experimental procedures for wave and pulse propagations is given by Hunter [23]. Techniques used in the analysis of the transient pulse propagation in the present investigation follow closely those given by Hunter.

The survey papers by Kolsky [24] and Hunter [23] provide a comprehensive review of publications in the area of wave propagation in viscoelastic materials prior to 1961. Several significant papers have been published since then: Chu [25] and Valanis [26] investigated the propagation and attenuation of waves in linear viscoelastic materials for which the relaxation function is known as a function of time and showed that "weak" (small) wave fronts propagate at a constant speed dependent only upon the "glassy" modulus of the material, that is, on the initial value of the relaxation function. The attenuation of these wave fronts is exponential in character and the attenuation rate depends only upon the initial value and initial slope of the relaxation function. Fisher and Gurtin [27] and Herrera and Gurtin [28] extended these results to include waves of finite amplitude propagating through anisotropic and inhomogeneous viscoelastic solids. But the initial value and initial slope of the relaxation function, necessary to experimentally apply the analytical results discussed above, cannot be directly obtained experimentally. This leads to difficulties in inverting the Laplace transform solutions for the shape and velocity of the propagating pulse as a function of position and time. For this reason the use of Fourier transform techniques and the complex modulus form of characterizing the material properties seems to be a more promising approach to wave propagation analysis.

Experimental work in the area of wave propagation in viscoelastic materials is limited. Kolsky [29] investigated the propagation of "short" mechanical pulses along rods of three different polymers. The pulses were applied to the ends of the rods by an explosive charge of approximately 2 microseconds duration. The experimental results were compared with pulse shapes predicted by numerical Fourier synthesis using the complex modulus form for describing the material behavior and a dirac-delta-function approximation to the input pulse. Norris [30] extended the work of Kolsky to the case of a much longer initially-applied stress pulse and the results showed good agreement between the experimental and computed wave shapes and velocities. Lifshitz and Kolsky [31] experimentally investigated the assumption, generally used in the application of the well-known correspondence principle, that the bulk modulus is real, whereas the shear modulus is complex. The results indicated that the loss tangent of the bulk modulus was approximately 20% of that of the shear modulus. This assumption was tested by measuring the propagation of a spherically-divergent stress pulse in a linear viscoelastic solid. Photoelastic techniques have been used by Dally [32], Daniel [33], and Arenz and Fourney [34] to study two-dimensional wave propagation in photo-viscoelastic model materials. Durelli [35] has determined the stress-strain curves at different strain rates in rubber-like materials by photoelastic techniques.

As noted above, most viscoelastic materials are linear for sufficiently small strains. In most polymers, e.g. polyethylene, the transition from linearity to nonlinearity is quite smooth. The problem is how to extend the theory to describe the nonlinearities which occur for large strains. In general, the experimental problem is made more complex in that the nonlinear material behavior is combined with nonlinear geometric effects due to large strains.

A general constitutive equation for viscoelastic materials (materials with memory) has been formulated and discussed by Green, Rivlin and Spencer [36, 37, 38]. They assume that the elongation of a specimen at time t depends on all previous values of the rate of loading to which the specimen has been subjected. That is, in the one dimensional case:

$$e(t) = F\left[\frac{d\sigma(\tau)}{d\tau}\right]_{\tau=-\infty}^{t} \qquad (2.1\text{-}2)$$

If the functional F is continuous and nonlinear, Frechet has shown [see 36] that the functional expression for the elongation can be represented to any degree of accuracy in the following manner:

$$e(t) = \int_{-\infty}^{t} J_1(t-\tau_1)\frac{d\sigma(\tau_1)}{d\tau_1}\, d\tau_1$$

$$+ \int_{-\infty}^{t}\int_{-\infty}^{t} J_2(t-\tau_1,t-\tau_2)\frac{d\sigma(\tau_1)}{d\tau_1}\,\frac{d\sigma(\tau_2)}{d\tau_2}\, d\tau_1 d\tau_2$$

$$+ \int_{-\infty}^{t}\int_{-\infty}^{t}\int_{-\infty}^{t} J_3(t-\tau_1,t-\tau_2,t-\tau_3)\frac{d\sigma(\tau_1)}{d\tau_1}\,\frac{d\sigma(\tau_2)}{d\tau_2}\,\frac{d\sigma(\tau_3)}{d\tau_3}\, d\tau_1 d\tau_2 d\tau_3$$

$$+ \ . \ . \ . \qquad (2.1\text{-}3)$$

If only the first term on the right is retained, this expression for e(t) reduces to the linear hereditary integral expression of the Boltzmann superposition principle [5]. Lockett [39] has extended the above development to the more general three-dimensional case and defined a series of experiments which are required to determine the twelve material functions which appear in the three-dimensional constitutive relations involving multiple integrals of the first, second and third orders. A minimum of 330 separate tests are required. Less ambitious experimental investigations for the one-dimensional case have been made by several investigators [40-44]. Multiple-integral representations of the third order, involving three material functions, have been successfully employed to describe the nonlinear creep and recovery behavior of several polymers.

Noll [45] and Coleman and Noll [46] have given a more general form of the constitutive equation based on thermodynamic considerations and a postulated principle of fading memory. Their constitutive equation is valid whenever the deformation is slow; hence it is essentially restricted to the quasistatic case. Some approximations [47, 48, 49] to this theory have been proposed for "short time" (dynamic) behavior. Lianis and DeHoff [48] proposed an approximate theory for small dynamic strains superposed on static large deformations in transversely-isotropic materials in which it is necessary to determine fifty kernels (material functions).

Because the complete specification of the nonlinear response is so difficult there has been some interest in the possibly-simpler problem of small increments superposed on a finite prestrained state.

1.3. Previous Work Leading to this Investigation

Previous investigations of the effect of prestrain upon the dynamic mechanical properties of viscoelastic materials are few. Biot [50] has shown that, on the basis of the linear theory of viscoelasticity, prestress (prestrain) influences longitudinal wave propagation only through its effect upon the magnitudes of the modulus and density of the material. The phenomenon must therefore be considered as being a nonlinear-material effect.

Hillier and Kolsky [1] have studied the propagation of continuous waves along 1 mm.-diameter filaments of polyethylene, neoprene and nylon at a frequency of 3000 cycles per second while the specimens were being elongated at a constant rate of strain, 0.0015 per second. Measurements of the phase velocity and some values of the damping factor were obtained for elongations up to approximately 140% for polyethylene and nylon and 500% for neoprene. Measurements at 1500 cps and 6000 cps were also recorded for undrawn filaments of polyethylene. All data were taken at 20°C. Their results showed an increase of the order of 100% in the dynamic modulus at 3000 cycles per second for elongations of 100%. Slight decreases in the values of the dynamic moduli of polyethylene and nylon were noted, however, at low strains, followed by a rapid rise. Correlation of the results with the molecular rearrangements which take place during large elongations were discussed. The experimental method and apparatus used in the present investigation is similar to that used by Hillier and Kolsky; it is discussed in Sections 2.2 and 2.3.

The influence of strain upon the dynamic properties of natural rubber has been studied by Mason [2] and of some synthetic rubbers by Hillier [3]. Mason recorded phase velocity and attenuation over a limited frequency range for a series of temperatures, and then used the time-temperature superposition principle (method of reduced variables), developed by Williams, Landel and Ferry [51], to extend this information over a wider frequency range at a single reference temperature. The results reported in both of these papers [2, 3] are similar to those reported by Hillier and Kolsky. For extensions up to 600% the dynamic modulus for some rubbers increased as much as two orders of magnitude. An initial decrease in the dynamic modulus with strain in the range of strain from zero to 50% was noted for some materials. The damping factor also varied considerably with strain.

The present study explores in greater detail the effect of moderate prestrains (up to 10%) upon the dynamic mechanical properties of low-density polyethylene. The results of the present study are compared to the above results and discussed in Section 2.5.

II. DETERMINATION OF MATERIAL PROPERTIES

2.1. Introduction

The engineering analysis of structures uses, in general, a system of equations that can be divided into two categories: one, the field equations and boundary conditions, which incorporate the geometry into the analysis, and two, the constitutive equations, which describe the fundamental mechanical relationship between load and deformation (stress and strain) for the material. This investigation is primarily concerned with the second category; therefore the field equations will be made as simple as possible so as to emphasize the constitutive relationship. The geometry of the material specimens was chosen to be a slender rod, and the frequencies and pulse rise-times are such that the assumption of one-dimensional analysis can be made.

The analysis for the method is presented in Section 2.2, and details of the experimental technique are given in the following section.

2.2. Method of Determining the Material Properties

A number of experimental methods are available for the measurement of the dynamic mechanical properties of polymers. Hillier [52] gives an excellent survey of available techniques up to 1961. Brown and Selway [53], Adkins [54] and Philbrick [55] have enlarged upon these techniques in recent years.

The method of measurement is essentially determined by the relevant frequency range desired. For purposes of correlation with Fourier transform techniques, the pertinent frequency range is that comprising the Fourier spectrum of the pulse. On the other hand, if a complete description of the material properties is required, from the rubbery range through the transition range and into the glassy range, probably no single technique will suffice. For instance, the transition region for polyethylene spans approximately eight decades of frequency (or time), and there is no available technique that will span this range.

The time-temperature superposition principle, using the method of reduced variables, as developed by Williams, Landel and Ferry [51], provides a means of extending the range of any one technique. In using this method the mechanical properties are determined in the usual manner over the available frequency (or time) range, but for a series of temperatures. The Williams-Landel-Ferry technique is then used to extend this information over a broad frequency (or time) range for a single reference temperature. The method assumes a single temperature-dependent dissipative mechanism over the range of the expanded frequency (or time) scale. Extensive temperature conditioning equipment is required in order to utilize this technique. In addition, the equipment used in the measurement technique itself must be capable of operating over the required temperature range.

A transient pulse analysis was made in the second part of this investigation. Therefore the properties were sought in the form of the complex modulus. Two general methods are available for this: resonance methods using short specimens, and sinusoidal traveling-wave methods. The wave-propagation method was used in this study, because preliminary experiments indicated that with the equipment available it would give more precise data. In the wave-propagation method, the parameters actually measured are the frequency-dependent phase velocity $c(\omega)$ and damping factor $\alpha(\omega)$. These two parameters are related to the complex modulus, discussed in Section 1.2, as follows:

$$c(\omega) = \left[\frac{E^*}{\rho}\right]^{1/2} \sec \frac{\delta}{2} \qquad (2.2\text{-}1a)$$

$$\alpha(\omega) = \frac{\omega}{c} \tan \frac{\delta}{2} \tag{2.2-1b}$$

where $(E^*)^2 = E_1^2 + E_2^2$ and $\tan \delta = E_2/E_1$. The derivation from which these relationships are taken is given below, beginning with equation (2.2-2).

The method used for determing the frequency dependent phase velocity $c(\omega)$ and damping factor $\alpha(\omega)$ for polyethylene was selected so that the frequency range of the material data spanned the Fourier spectrum of the impact-induced strain pulses used in Part III. This range was of the order of the audio frequency range.

The parameters $c(\omega)$ and $\alpha(\omega)$ were determined for a series of prestrain elongations up to approximately 10%. It was assumed that the material undergoes a linear dynamic response to small dynamic increments in the neighborhood of a state of static prestrain. This assumption was checked experimentally during the course of the experimental investigation. The technique of measurement was first developed by Ballon and Silverman [56], and has been used by Hillier and Kolsky [1], Mason [2] and Norris [57]. The theory is thoroughly presented in the paper by Hillier and Kolsky, including the effect of reflection due to the measuring transducer. A summary of the method will be given here:

The equations necessary to describe uniaxial wave propagation in a slender viscoelastic rod are the equation of motion

$$\frac{\partial \sigma}{\partial x} = \rho \frac{\partial^2 u}{\partial t^2} \quad , \qquad (2.2\text{-}2)$$

the strain displacement relation

$$\varepsilon = \frac{\partial u}{\partial x} \quad , \qquad (2.2\text{-}3)$$

the constitutive equation, as given in complex modulus form by equation (1.2-1):

$$\frac{\sigma}{\varepsilon} = E(i\omega) = E^* e^{i\delta} \quad ,$$

and the associated boundary and initial conditions. Substituting (1.2-1) and (2.2-3) into (2.2-2) gives:

$$\frac{\partial^2 u}{\partial x^2} = \frac{\rho}{E} \frac{\partial^2 u}{\partial t^2} \quad . \qquad (2.2\text{-}4)$$

For sinusoidal time dependence, the solution to (2.2-4) is taken in the form

$$u(x,t) = v(x)\ e^{i\omega t} \quad . \qquad (2.2\text{-}5)$$

The reduced equation becomes

$$\frac{\partial^2 v}{\partial x^2} - \lambda^2 v = 0 \quad , \qquad (2.2\text{-}6)$$

where

$$\lambda^2 = \frac{\rho(i\omega)^2}{E^* e^{i\delta}} \qquad (2.2\text{-}7)$$

If the rod is taken to be semi-infinite in length and stress-free on all boundaries except at the accessible end x = 0, where

$$u(0,t) = U_\circ \; e^{i\omega t} \quad , \qquad (2.2\text{-}8)$$

then the solution to the reduced equation (2.2-6) for the outgoing wave is

$$v(x) = U_\circ \; e^{-\lambda x} \qquad (2.2\text{-}9)$$

where $\lambda = \alpha + ik$ is a complex function of ω. The complete solution is

$$u(x,t) = U_\circ \; e^{-\alpha x} \; e^{i\omega[t-(x/c)]} \qquad (2.2\text{-}10)$$

where

$$k = \omega/c \quad . \qquad (2.2\text{-}11)$$

The phase velocity c and damping factor α can be related to the complex modulus and ω by equation (2.2-7):

$$\lambda = \alpha + i\frac{\omega}{c} = \left[\frac{\rho(i\omega)^2}{E^* e^{i\delta}}\right]^{1/2}$$

$$= \frac{\omega}{[E^*/\rho]^{1/2}} \left(\sin\frac{\delta}{2} + i\cos\frac{\delta}{2}\right)$$

$$= \frac{\omega}{c}\tan\frac{\delta}{2} + i\,\frac{\omega}{[E^*/\rho]^{1/2}\ \sec\delta/2} \quad . \qquad (2.2\text{-}12)$$

The equations (2.2-1) relating the phase velocity c and damping factor α to the complex modulus follow from equation (2.2-12).

Consider a laboratory setup where a steady sinusoidal displacement given by equation (2.2-8) is applied to one end of a long slender rod of a viscoelastic material. If the material has sufficient damping and the rod is sufficiently long so that there are essentially no waves reflecting from the terminated far end, then the rod may be considered semi-infinite in length. In this case the displacement transmitted past any section at a distance x from the driven end will be given by equation (2.2-10). If a transducer is brought into contact with the rod at a distance ℓ from the driven end, the wave reflected from the transducer will be

$$u_r(x,t) = -mU_o \, e^{-\alpha(2\ell-x)} e^{i\omega(t-\frac{2\ell-x}{c})} \quad , \qquad (2.2\text{-}13)$$

for $0 \leq x \leq \ell$, where "m" is the reflection coefficient. The measured displacement at any point $0 \leq x \leq \ell$ is then the sum of the transmitted displacement u and the reflected displacement u_r. In particular, the measured displacement at the input end is

$$u_i(0,t) = u(0,t) + u_r(0,t) \quad , \qquad (2.2\text{-}14)$$

and the measured displacement at the transducer is

$$u_\ell(\ell,t) = u(\ell,t) + u_r(\ell,t) \quad . \qquad (2.2\text{-}15)$$

Experimental measurements will give the input amplitude A, the amplitude B at the transducer (where $x=\ell$), and the phase angle θ by which the wave at $x=\ell$ lags behind the input wave. From the relationship

$$\frac{Ae^{i\omega t}}{Be^{i(\omega t-\theta)}} \equiv Re^{i\theta} = \frac{u_i(0,t)}{u_\ell(\ell,t)} \qquad (2.2\text{-}16)$$

the following equation can be derived:

$$\tan\theta = \frac{(1+me^{-2\alpha\ell})}{(1-me^{-2\alpha\ell})} \tan\frac{\omega\ell}{c} \qquad (2.2\text{-}17)$$

If the term $m[\exp(-2\alpha\ell)]$ is sufficiently small, this expression may be written approximately as $\tan \frac{\omega\ell}{c} = \tan\theta$ from which the phase velocity is

$$c = \frac{\omega\ell}{\theta} \tag{2.2-18}$$

The curve of phase angle θ as a function of distance ℓ expressed by equation (2.2-16) shows a damped oscillation superimposed upon a straight line of slope k, as seen in Figure 2.4-5. For sufficiently large values of ℓ an accurate determination of the slope can be obtained. Hillier [52] claims that an accuracy of ±1% can be obtained.

A second expression derivable from the complex equation (2.2-15) is

$$R \equiv \frac{B}{A} = \frac{(1-m)\ e^{-\alpha\ell}}{[1-2me^{-2\alpha\ell}\cos\frac{\omega\ell}{c} + m^2e^{-4\alpha\ell}]^{1/2}} \tag{2.2-19}$$

from which the damping factor may be determined. If α is sufficiently large, then equation (2.2-19) can be written approximately as:

$$\ell n\ (\frac{B}{A}) = -\alpha\ell \tag{2.2-20}$$

The graph of the logarithm of the amplitude ratio as a function of position ℓ will give the value of the damping factor directly as the slope of the straight line. Again, as shown in Figure 2.4-6, damped oscillations are superimposed on the straight line. If points are selected where $\frac{\omega \ell}{c} = \frac{\pi}{2}, \frac{3\pi}{2}, \frac{5\pi}{2}, \ldots,$ then the middle term in the denominator is rendered zero (the last term is much less than unity as it stands) and the significance of the oscillation is reduced. The phase velocity c and the damping factor α, when determined for a series of selected frequencies, provide a complete description of the mechanical properties of the material over that frequency range. Repeating this method for a series of longitudinal prestrains of the material then provides the desired description of the material as a function of both frequency and prestrain. In effect, an "incremental" complex modulus is determined as a function of prestrain.

Experimental details of this program are given in Section 2.3. It should be kept in mind that this method is only valid provided the assumption of one-dimensional theory holds, that is, provided the diameter (transverse characteristic dimension) of the rod is small compared to the wavelength of the traveling wave.

2.3. Details of the Experimental Technique

2.3.1. Specimens

One-eighth-inch diameter rods of low-density unoriented polyethylene were used in this investigation.

The material was obtained from Allied Resinous Products, Inc., Conneaut, Ohio, under the classification of "polyolefin welding rod."

The selection of this material was based on several factors. The complex modulus has a considerable variation over the frequency range comprising the Fourier spectrum of the pulse utilized in the second part of this investigation. That variation occurs when the material is at room temperature, thus permitting the material properties to be determined and the subsequent pulse propagation experiments to be conducted at room temperature. While a considerable amount of information has been published for polyethylene, there evidently has been very little investigation of the dependence of the dynamic mechanical properties of polyethylene upon prestrain in the range of strain considered here. The material-characterization experiments by continuous-waves and the pulse-propagation experiments could be conducted using specimens of the same geometry, thereby minimizing any effects that specimen geometry may have on the results and comparison.

2.3.2. Continuous Wave Source

The vibration driver used was an MB Electronics Model EA-1500 Vibration Exciter, with matching power amplifier. The driver has a 35-pound force-amplitude output capability. The frequency range of this unit is 5 to 15000 cycles per second, which was sufficient to cover the frequency range comprising the Fourier spectrum of the pulse used in the second part of this investigation. Since the flexural supports of the moving element (armature) of the exciter were not sufficient to support the static load on the polyethylene rod, an auxiliary flexural support was constructed. The auxiliary support is essentially a beam with fixed ends, which is driven transversely at midspan to introduce the sinusoidal wave into the polyethylene rod. The flexural stiffness of the beam was made large enough to support the static load but "soft" enough to permit the required flexural amplitude when driven at midspan. The complete support fixture also incorporates a provision for alignment of the exciter with the beam to prevent damage to the exciter armature during operation. The entire fixture was mounted on a lathe bed, along with the displacement-measuring transducers. Figure 2.3-3 is a photograph of the complete test apparatus.

The method of attaching the polyethylene rod at the driven end is shown in Figure 2.3-1. The end of the polyethylene rod was upset by heating it to approximately 100°C and applying an axial compressive load while it cooled. A heat sink was applied around all but approximately one inch of the end of the polyethylene rod to prevent altering of the material properties. The heat sink consisted of two pieces of aluminum bar stock, 1-inch

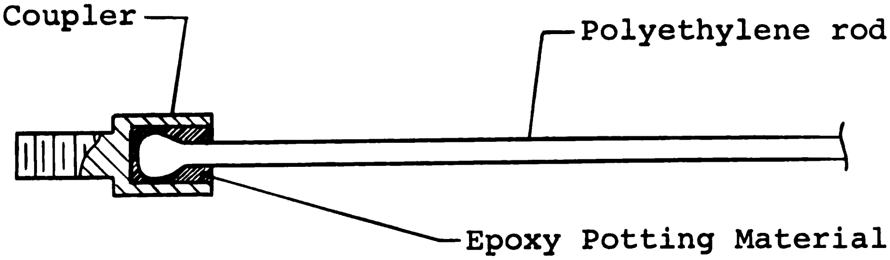

Figure 2.3-1. Fixture for Attaching the Polyethylene Rod at the Driven End

by 1-1/2-inch by 4-inches long, which were clamped together. A 1/8-inch diameter hole was drilled along the length of the interface between the two bars to hold the polyethylene rod while the end was being upset. The bars were then separated to release the rod after the bulbous end had been formed. The bulbous end of the rod was then embedded in the metal coupler with a room-temperature-setting epoxy. This provided a fixture that would support the static axial load on the polyethylene rod without causing it to fail by "necking" and, at the same time, would transmit the oscillatory force into the rod without apparent distortion.

2.3.3. Static Prestrain

The prestrain elongation was induced in the rod by passing the far end over a sponge-rubber-covered pulley and applying a dead-weight load. The material was allowed to creep until the desired elongation was attained and then it was clamped. The pulley was positioned at various distances from the driven end; up to 40 feet was required at low frequencies to effectively eliminate the effect of wave reflection from the far end, so that the displacements measured were essentially those in a semi-infinite rod. The wave-reflection problem is discussed further in the following section.

2.3.4. Displacement-Measuring Transducers

Two crystal phonograph cartridges, Astatic Model 62-1, were used as displacement-measuring transducers. The apparatus for positioning each transducer along the lathe-bed way is shown in the photograph of Figure 2.3-3. The device utilizes a microscope stage for adjusting the transducer into contact with the polyethylene rod. An extension for the lathe-bed way was constructed to permit a total transducer travel of 180 inches.

These transducers were calibrated with reference to an accelerometer, the output of which was continuously integrated, through two operational amplifiers in series, to give a displacement signal. The transducers were found to produce an output voltage linear with displacement amplitude over the range of frequencies and amplitudes employed in this test. Calibration curves are shown in Figure 2.3-2. The standard stylus delivered with the transducer was used; the pointed stylus was found to

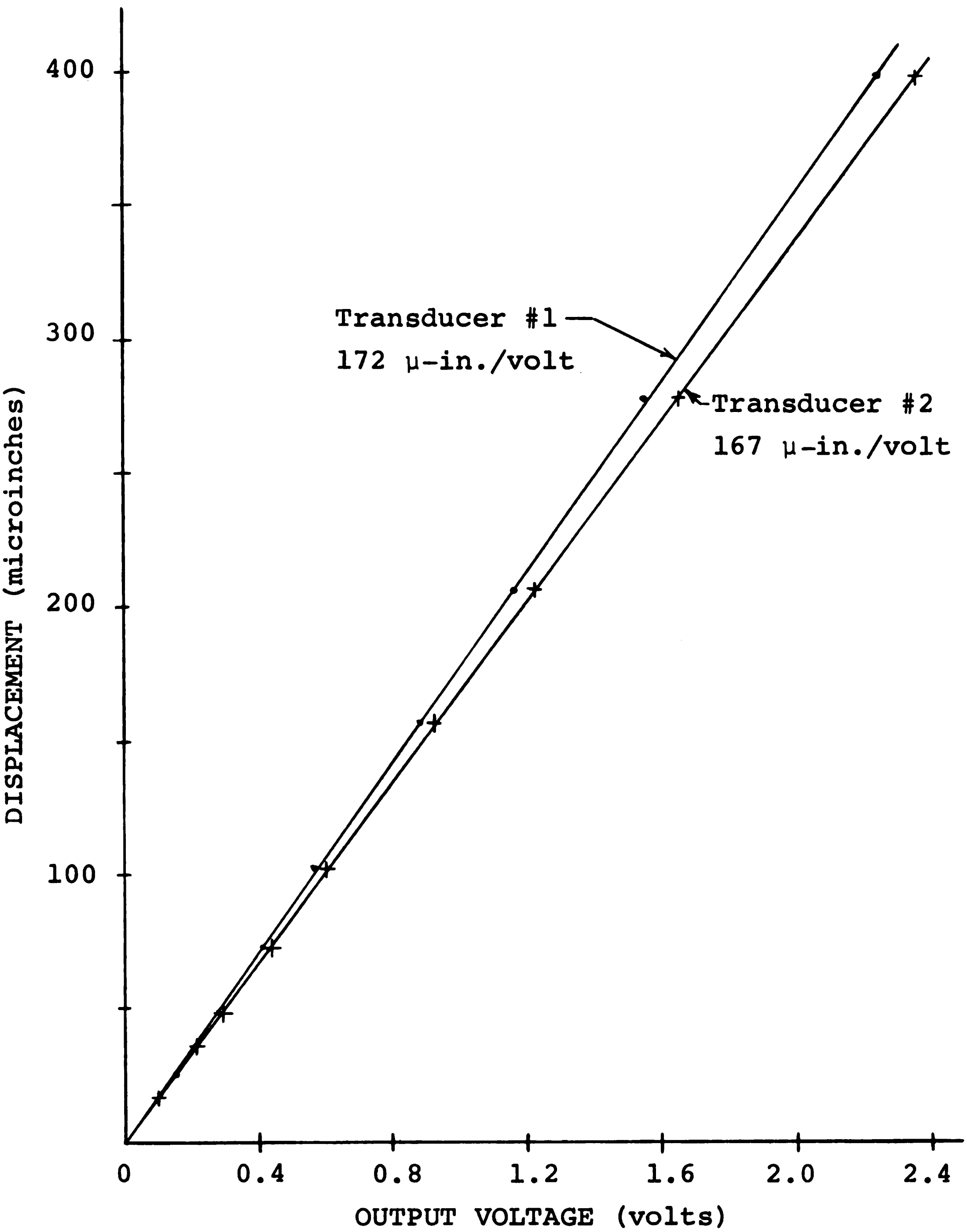

Figure 2.3-2. Displacement - Voltage Calibration Curves for the Displacement Measuring Transducers, Astatic Model 62-1 Crystal Phonograph Cartridges. The calibration was performed using sinusoidal displacements.

provide reliable contact with the polyethylene rod. After sufficient contact pressure was established (approximately 4 grams.) to provide a visibly-undistorted signal on the monitoring oscilloscope, the transducer output was essentially independent of pressure over a broad range of contact pressure. Nevertheless, the transducer output signals were visually monitored throughout the tests.

The effect of wave reflection from the transducer was checked experimentally. One transducer was brought into contact with the polyethylene rod at an arbitrary position and the signal amplitude and phase relative to the driver observed. The second transducer, when contacted with the rod at various distances along the rod, produced no significant change in the output of the first transducer. This was interpreted as an indication that the transducer reflection coefficient "m" in equation (2.2-12) was small. Nevertheless, a small oscillation of the phase shift angle θ versus position ℓ was observed about a straight line in the experimental results at low frequencies and in the results for attenuation over a larger frequency range. See Figures 2.4-5 and 2.4-6.

The assumption of a semi-infinite rod was also checked experimentally. The distance of the far-end pulley from the driven end was adjusted so that the measured amplitude at several points along the rod in the vicinity of the pulley was less than 10% of the input amplitude.

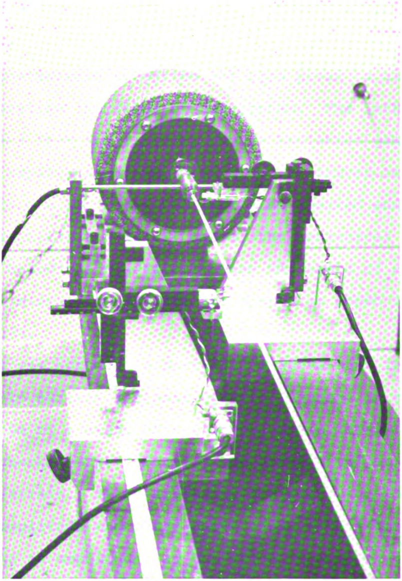

Figure 2.3-3. The Driver, Load Support Device and Transducers as Mounted on the Lathe Bed

The amplitude of the reflected wave at the input end would then be less than 1%. This was easily accomplished for all frequencies except the two lowest frequencies used in this test, for which the 40-foot length of the laboratory was the limiting factor.

Considerable attention was also given to the problem of vibration isolation of the system. The lathe bed was isolated from the floor by rubber isolation pads. Vibration amplitudes transmitted from the driver to the transducers via the lathe bed were also checked and found to be insignificant. In all cases, the mechanical noise level was below the electrical noise threshold of approximately 30 microvolts RMS for the system as shown in Figure 2.3-4.

It was assumed in Section 2.2 above that the material would exhibit a linear dynamic response in the neighborhood of a state of static prestrain. This assumption was checked experimentally for several values of static prestrain. At an arbitrary frequency the dynamic response amplitude and phase shift angle were recorded for a range of amplitudes at the driven end. No significant nonlinearity was observed over the range of dynamic amplitudes used in this study up to 0.1% dynamic strain.

The following section summarizes the experimental setup and procedure of the study.

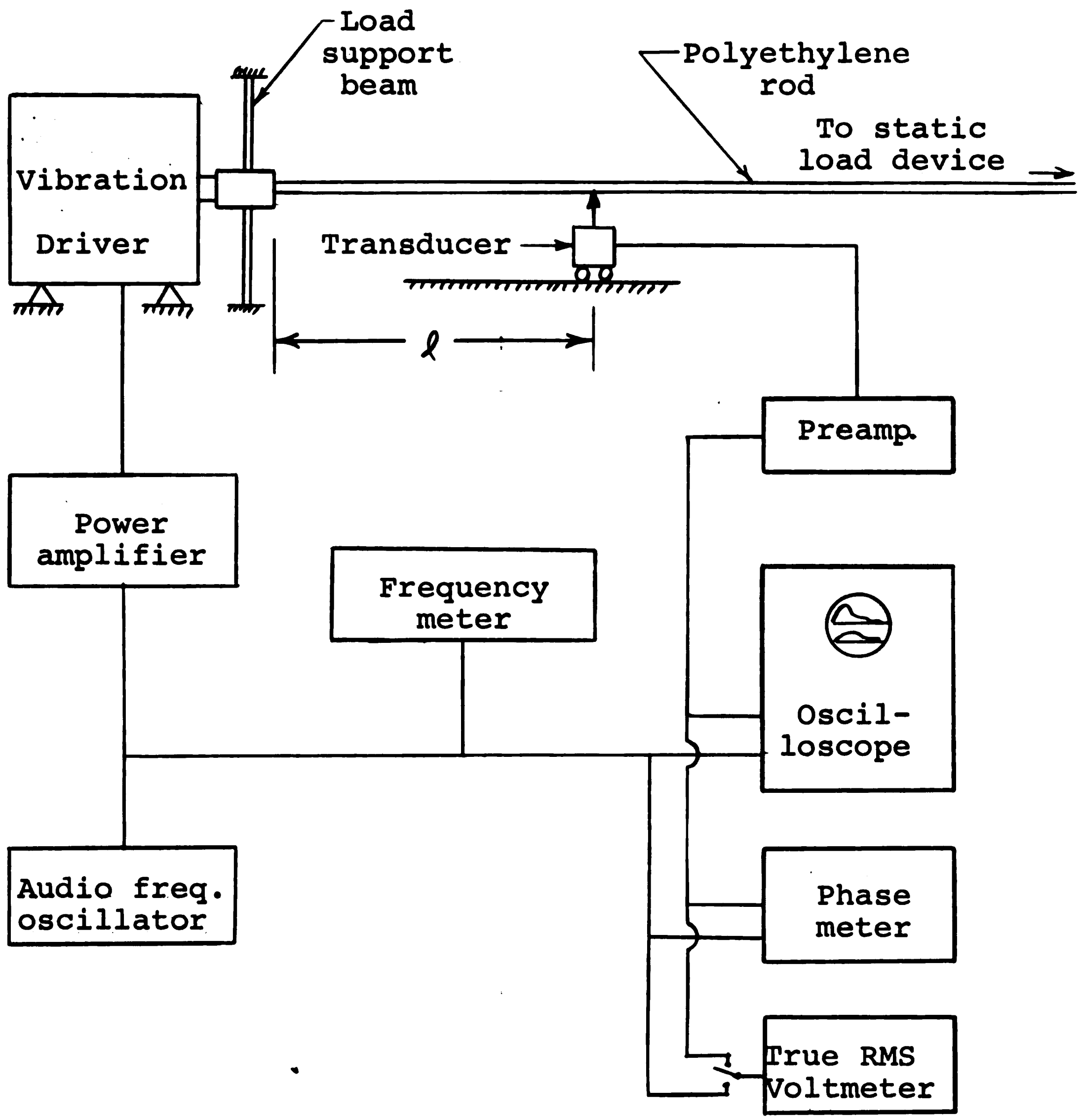

Figure 2.3-4. Schematic Diagram of the Experimental Apparatus Used for Material Property Measurements.

2.3.5. Experimental Setup and Procedure

A schematic diagram of the complete experimental apparatus used for measuring the material properties is given in Figure 2.3-4. Figure 2.3-3 is a photograph of the complete test apparatus.

The following specific items of equipment were used in this setup, as discussed in detail above:

1. MB Electronics Model EA-1500 Vibration Exciter with matching 125VA Power Amplifier.
2. Hewlett-Packard Model 200CD Sine Wave Signal Generator.
3. Hewlett-Packard Model 3734A Frequency Meter.
4. Acton Laboratories Type 320-AB Phase Meter.
5. Ballantine Laboratories Model 320 True Root-Mean-Square Voltmeter.
6. Tektronix Type 0 Preamplifier.
7. Tektronix Type 532 Oscilloscope.
8. Astatic Model 62-1 crystal phonograph cartridge.

The following experimental procedure was used for conducting the continuous-wave tests:

a. The material was received in coil form. Required lengths were laid out in a straight, flat position and allowed to relax in this form for a minimum of 24 hours at room temperature.

b. The equipment was turned on and allowed to warm up and stabilize.

c. The polyethylene rod was elongated a specified amount and then clamped at the far end. The initial elongation was 0.25%, sufficient to hold the rod in position for conducting the tests.

d. The desired frequency and amplitude were set on the signal generator and power amplifier.

e. The phase and amplitude of the wave in the rod were detected by the transducer and readings of the resulting phase and RMS voltage were recorded at successive positions along the rod.

f. Setps d. and e. were repeated for the complete frequency range at the given level of static elongation.

g. Another increment of prestrain elongation was applied. This was accomplished by applying an increment of load at the far end of the rod and permitting it to creep until the rate of creep became sufficiently slow, and then clamping the end.

h. Steps d. through g. were repeated for successively increasing levels of prestrain until the maximum level was completed.

In some instances data was taken for successively decreasing levels of prestrain. This data deviated from that obtained by the above procedure of successively increasing prestrain as is noted in the experimental results in Section 2.4.

2.4. Experimental Results

All of the tests were conducted at an ambient temperature of 72°F ± 1°.

Typical graphs showing the phase shift angle and attenuation as a function of the distance along the rod are given in Figures 2.4-5 and 2.4-6, respectively. These figures show the results for 0.25% and 8.0% elongation. These results are typical of the results obtained over the complete frequency range: the phase velocity decreases with increasing prestrain and the damping increases with increasing prestrain in the range of prestrains used in this study. The slope of the straight line of phase shift angle θ versus distance ℓ in Figure 2.4-5 gives the wave number $k = \omega/c$, as given by equation (2.2-11). The slope of the straight line of $\ln(A/B)$ versus distance in Figure 2.4-6 gives the damping factor α, as given by equation (2.2-20).

The phase data was reproducible within 1%, both for a given specimen and for several specimens cut from the same lot of material. The attenuation data, on the other hand, exhibited as much as 10% scatter at some points (see Figure 2.4-6). In general the amount of scatter decreased with increasing frequency. The attenuation data was uniformly scattered about a straight line faired through the data. In the lower-frequency data an

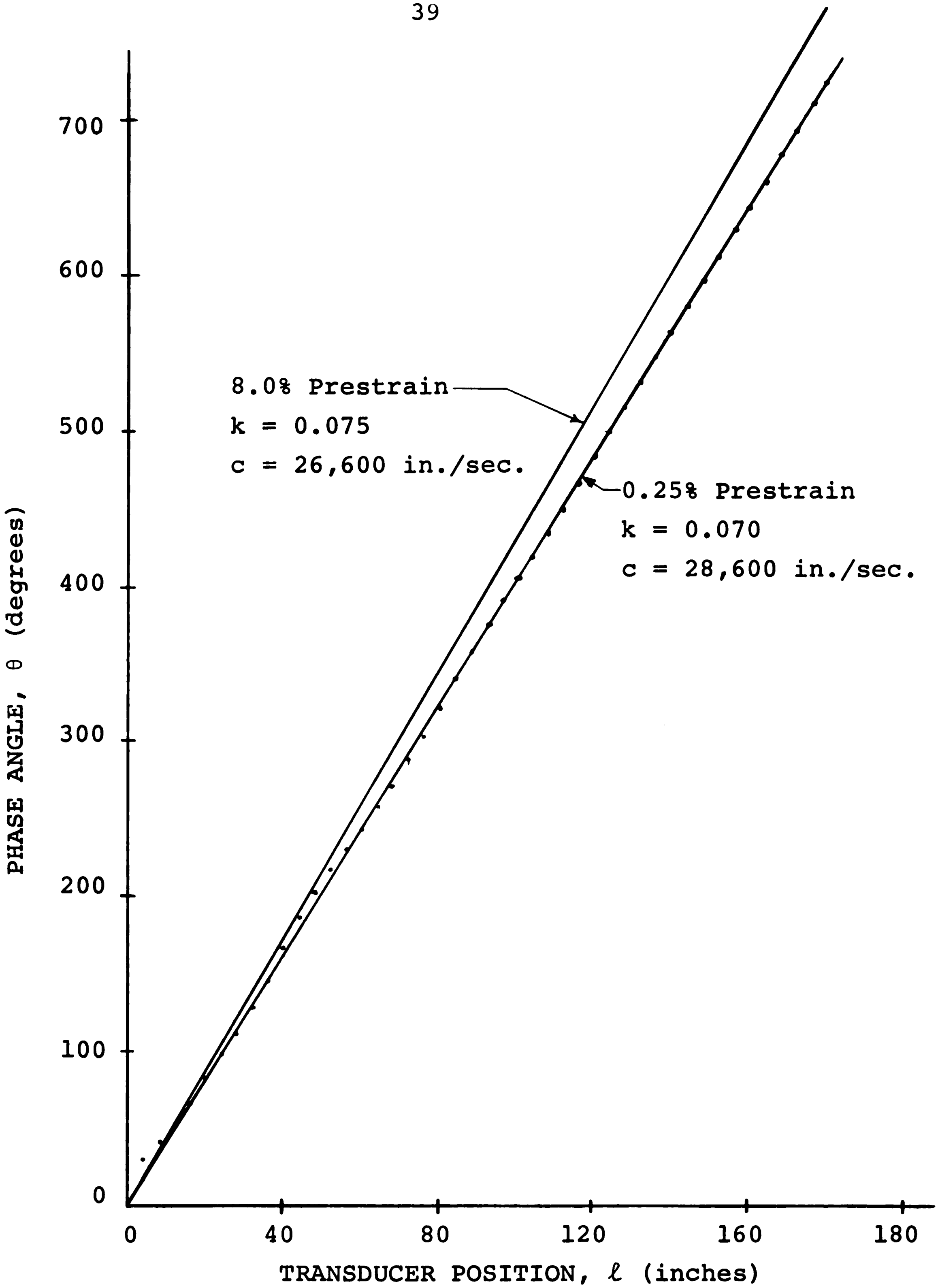

Figure 2.4-5. Typical plot of data for Phase Angle θ Versus Transducer Position ℓ (for $\omega = 2000$ per second). The slope of the straight line is $k = \omega/c$. Experimental points are shown for 0.25% prestrain.

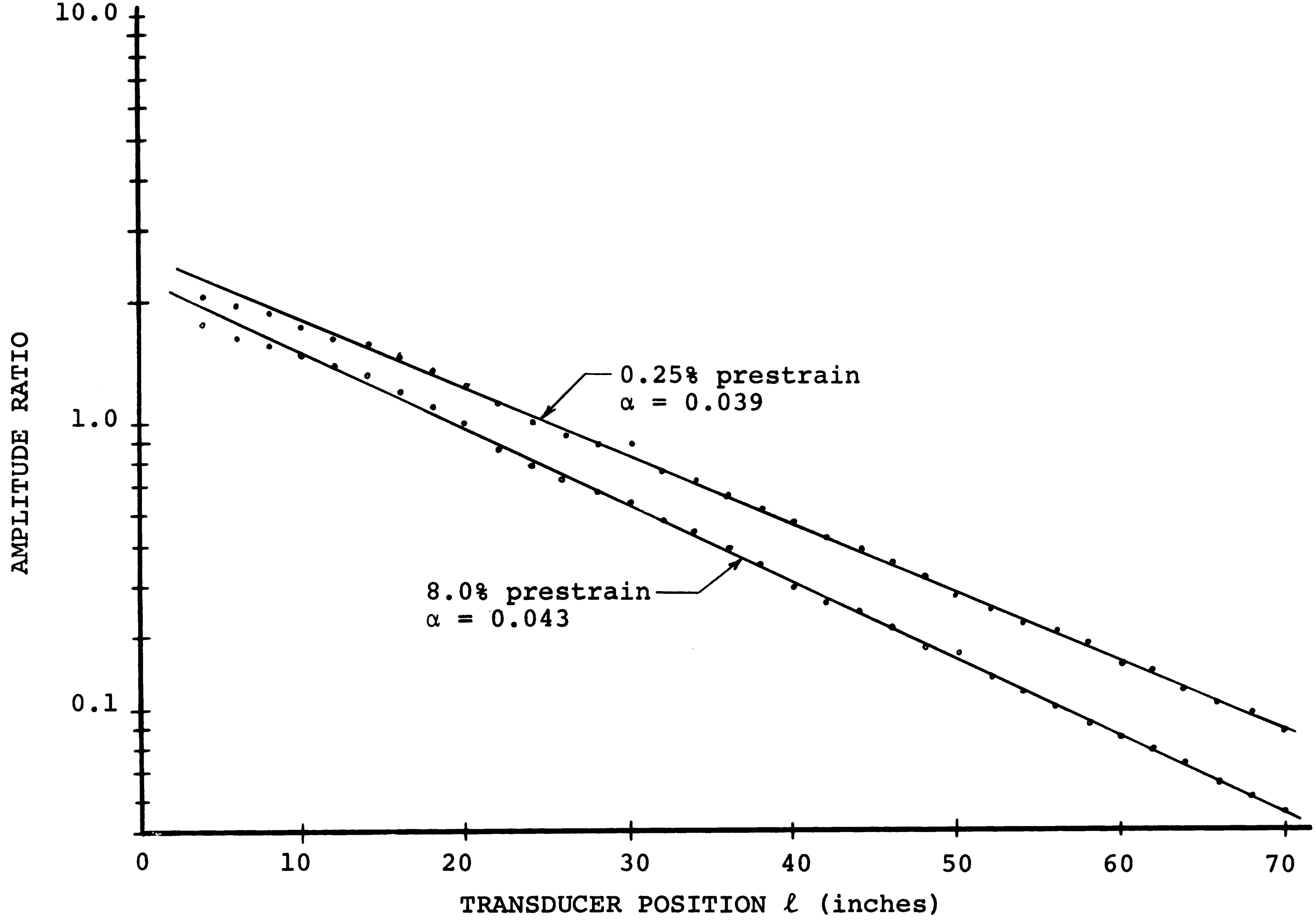

Figure 2.4-6. Typical Plot of Data for Amplitude Ratio A/B versus Transducer Position ℓ (for ω = 20,000 per second). The slope of the straight line gives the damping factor α.

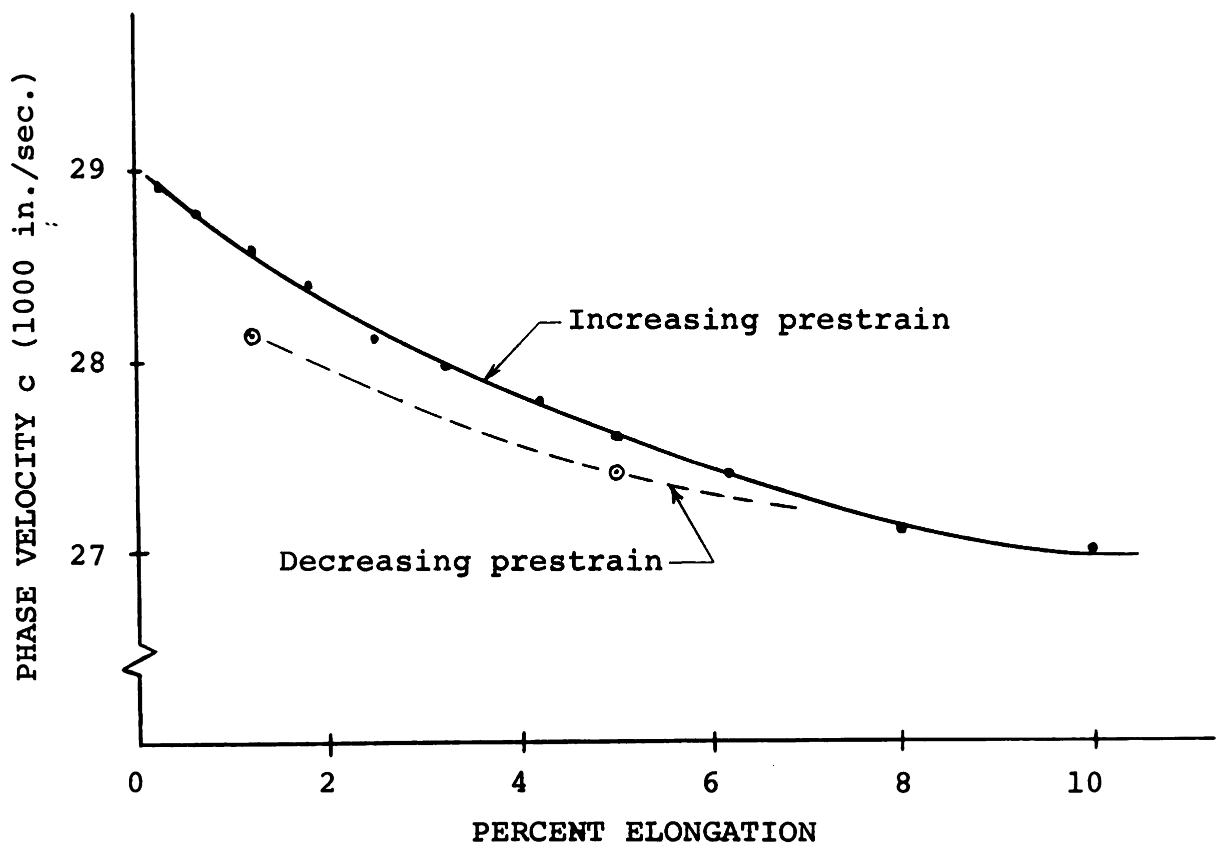

Figure 2.4-7. Phase Velocity Versus Percent Elongation at a Circular Frequency ω = 3000 per second

oscillation superimposed on this straight line was observed. Reliable attenuation data could not be obtained for ω less than approximately 5000 per second.

Figure 2.4-7 shows the change in phase velocity as a function of the percent elongation. This data was obtained for ω = 3000 per second by stationing the transducer at ℓ = 100 inches and recording the phase and amplitude of the transmitted wave as a function of the elongation. Similar curves were obtained for other values of ω; the same general form of curve and approximately the same percentage change was exhibited for each ω. The results for phase velocity as a function of frequency for the complete series of tests are given in Figures 2.4-8a and 2.4-8b for elongations of 0.25% and 8.0%. The results are displayed on a linear frequency scale in Figure 2.4-8a to emphasize the essential uniformity of the shift in phase velocity with prestrain. The logarithmic frequency scale used in Figure 2.4-8b suggests the form of the equation for the frequency-dependent phase velocity given in equations (2.4-1) and (2.4-2) below. The equation for the upper curve in Figure 2.4-8a, for 0.25% prestrain, is:

$$c(\omega) = \begin{cases} 20{,}700+2375 \log_{10}\omega, & \omega \leq 80{,}000 \text{ sec.}^{-1} \\ 32{,}400 \text{ (constant)}, & \omega > 80{,}000 \text{ sec.}^{-1} \end{cases} \tag{2.4-1}$$

And the equation for the lower curve, for 8.0% prestrain, is:

$$c(\omega) = \begin{cases} 16{,}290+3140 \log_{10}\omega, & \omega \leq 60{,}000 \text{ sec.}^{-1} \\ 31{,}450 \text{ (constant)}, & \omega > 60{,}000 \text{ sec.}^{-1} \end{cases}$$

(2.4-2)

The results for attenuation are summarized in Figure 2.4-9. The damping factor is essentially proportional to the frequency over the frequency range considered and can be expressed as follows:

$$\alpha(\omega) = d\omega \quad . \qquad (2.4\text{-}3)$$

For 0.25% prestrain $d = 2.17 \times 10^{-6}$ sec./in., and for 8.0% prestrain $d = 2.68 \times 10^{-6}$ sec./in.

All of the data as presented above was recorded for successive positive increments of prestrain elongation, as noted in the experimental procedure, Section 2.3.5. No negative increments (contractions) from any state of elongation was permitted during the tests. On completion of the tests in some specimens, the phase was recorded at a few states of elongation as recovery (contraction) occurred. A typical record is given by the dashed line in Figure 2.4-7. The phase velocity during recovery is offset

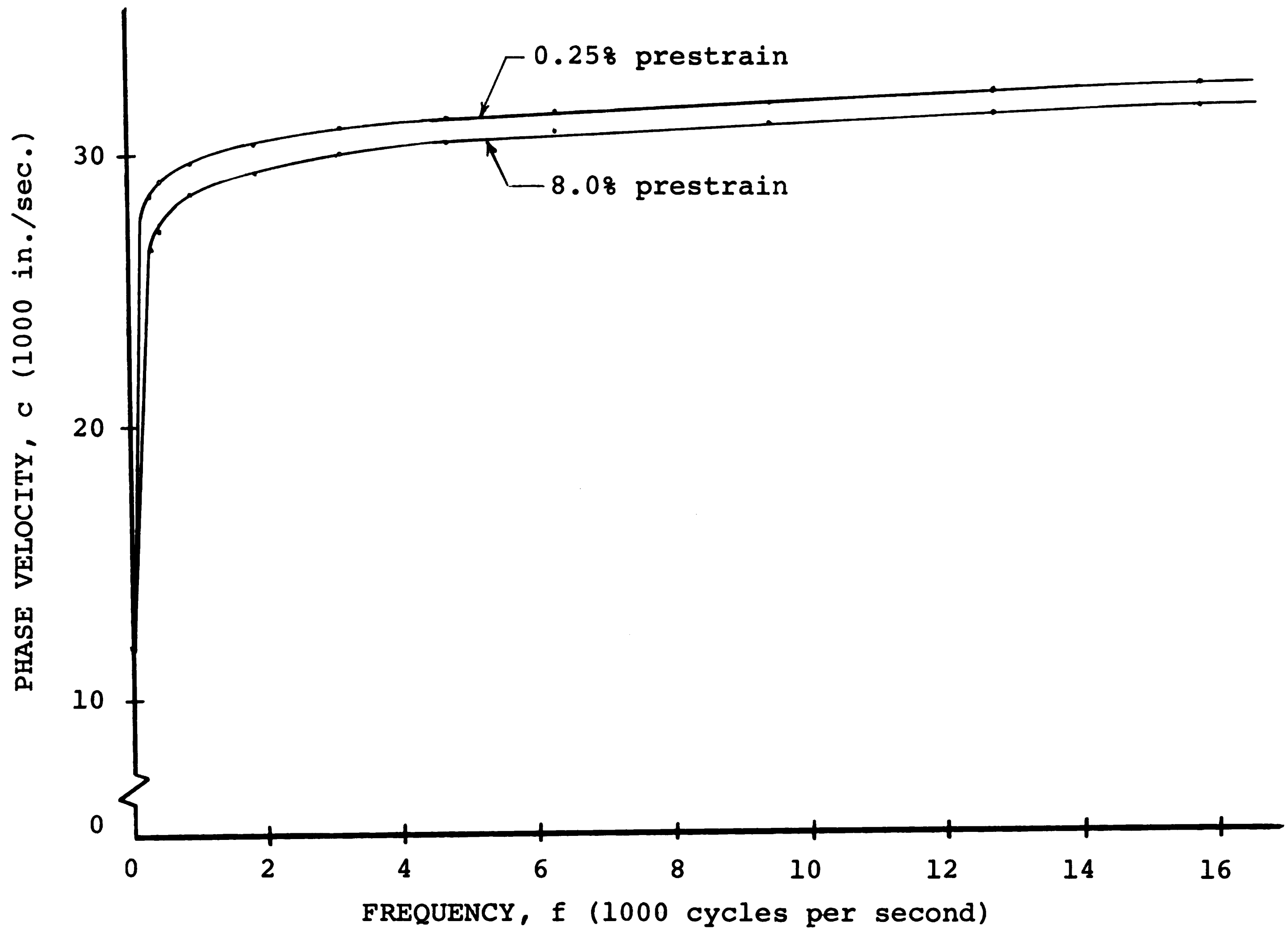

Figure 2.4-8a. Phase Velocity c versus Frequency f.

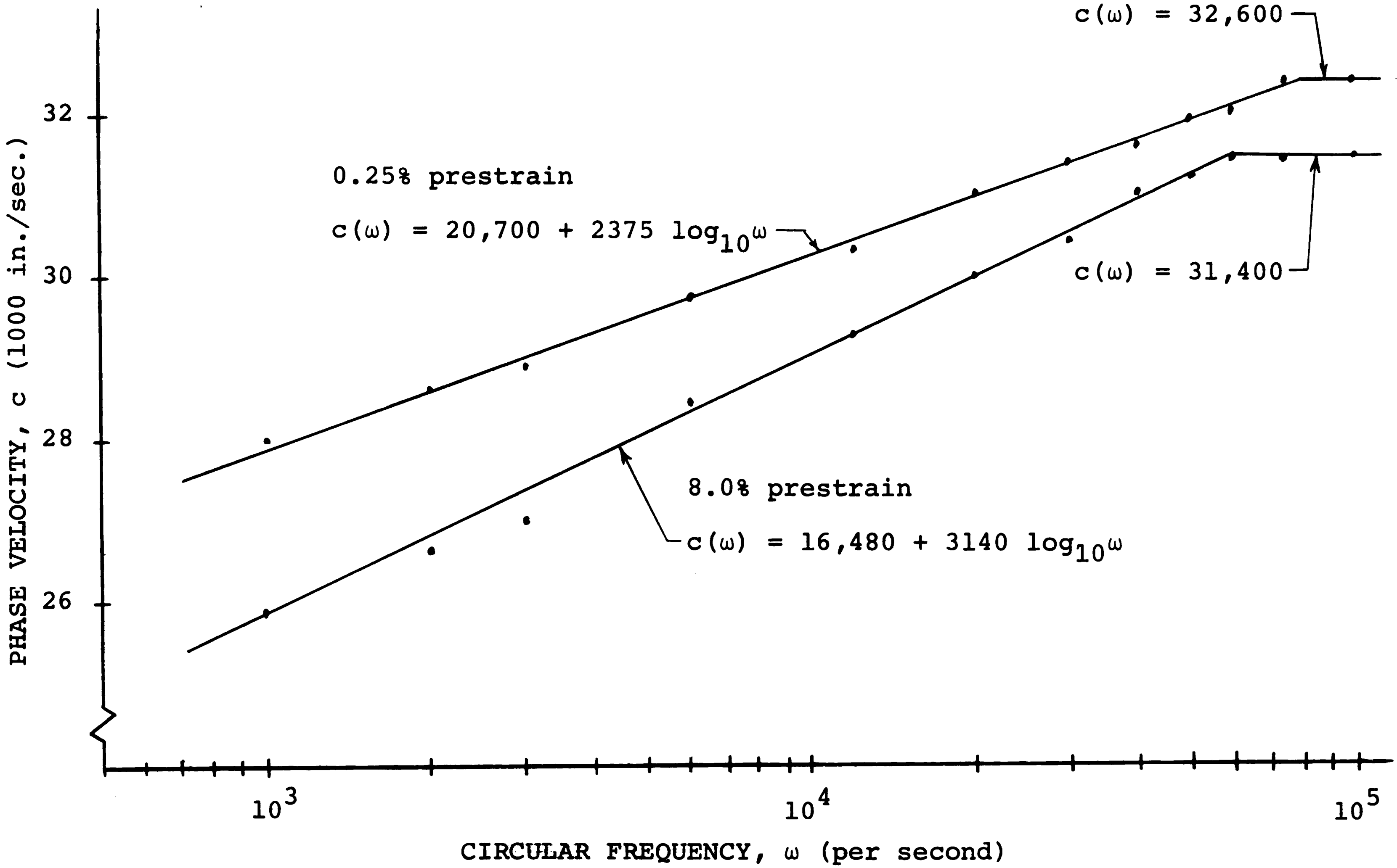

Figure 2.4-8b. Phase Velocity c versus Circular Frequency ω.

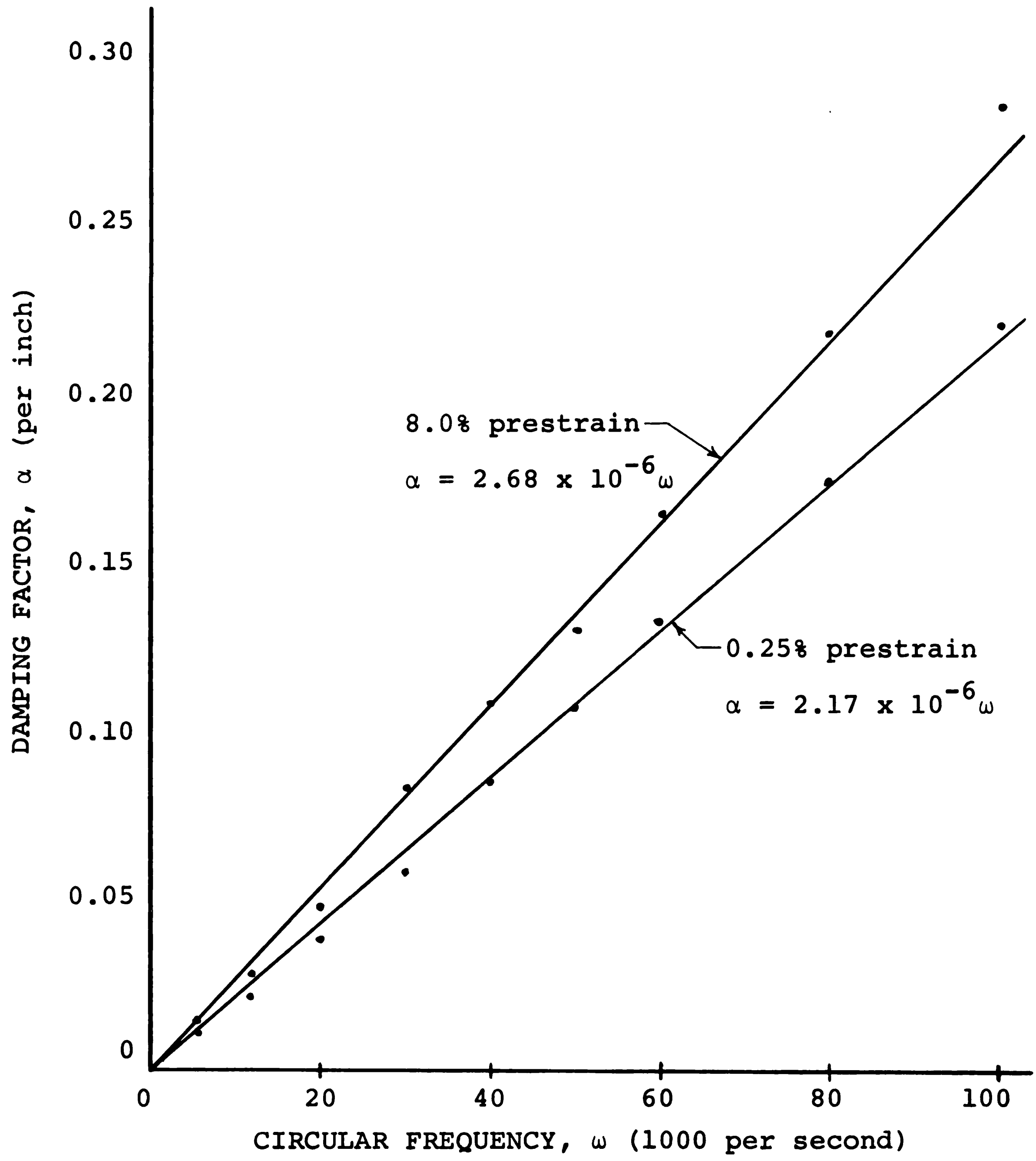

Figure 2.4-9. Damping Factor α versus the Circular Frequency ω. The data is approximated by straight line of the form $\alpha = d\omega$.

from that recorded for increasing elongation. Complete recovery of the elongation did not occur; approximately 1.0% strain remained after a minimum of 4 hours at no load.

There was no significant change in the phase or amplitude ratio due to the stress relaxation while tests were conducted at each level of elongation.

2.5. Discussion of Results

It should be reiterated here that in this study of the influence of prestrain upon the dynamic mechanical properties of polyethylene, the attitude has been to regard each quasistatic elongation as producing a new material, and consequently, to determine the "incremental" complex modulus as a function of frequency at each level of prestrain. The dynamic mechanical properties were determined in the form of the frequency-dependent phase velocity $c(\omega)$ and damping factor $\alpha(\omega)$, which together are equivalent to the complex modulus, the defining relationship given by equations (2.2-1).

The values obtained in this study for phase velocity in low-density polyethylene at 0.25% prestrain are compared in Table 2.4-1 with values given by Hillier and Kolsky [1] and Norris [57] for "unstretched" specimens of polyethylene, at three frequencies for which comparable data is available. The damping increased with frequency in all cases; for an approximate equation for damping in the form $\alpha(\omega) = d\omega$ (see equation 2.4-3), comparative values of the coefficient d are given in Table 2.4-1 also. Composite results of this Part II, as given in Figure 2.4-8 and 2.4-9 show that the phase velocity $c(\omega)$ decreases with increasing prestrain and the damping factor $c(\omega)$ increases with increasing prestrain, in the range of prestrain up to 10% as used in this investigation. Figure 2.4-7 shows the typical smooth manner in which the phase velocity decreases with prestrain. The results further indicate a relatively uniform shift of phase velocity with prestrain over the audio frequency range used in this study. All of this data is for a temperature of 72°F ± 1°.

These results are in good agreement with and extend the results given by other investigators. Data reported by Hillier and Kolsky [1] for phase velocity versus strain at a single frequency, 3000 cps, and at a temperature of 68°F, indicates a 2% decrease in the phase velocity at 10% prestrain (followed by a rapid rise of 300% as the strain was increased to 140%). The results of the present investigation show approximately 4% decrease in $c(\omega)$ at the same frequency for 8% prestrain. Hillier and Kolsky give no data on the effect of prestrain upon the damping factor for polyethylene.

TABLE 2.4-1.

COMPARISON OF DATA FOR PHASE VELOCITY AND DAMPING FACTOR FOR "UNPRESTRAINED" POLYETHYLENE

Frequency		Hillier & Kolsky [1]	Norris [30]	Present Study
		Phase Velocity, c (in./sec.)		
f(cps)	$\omega(\text{sec}^{-1})$			
1500	9,400	29,300	26,000	30,000
3000	18,800	30,800	27,130	30,900
6000	37,600	32,000	27,910	31,600
		Damping Factor ($\alpha = d\omega$)		
$d(10^{-6}$ sec./in.)		1.62	2.73	2.17

A similar decrease in the phase velocity for nylon for strains up to 10% has been given by Hillier and Kolsky [1] and for natural rubber by Hillier [3] and Mason [2]. On the other hand, data reported for neoprene [1] and other synthetic rubbers [3] exhibit no such initial decrease in phase velocity with prestrain.

Mason [2] reported an initial rise in the loss tangent ($\tan \delta = E_2/E_1$) for natural rubber for prestrains up to 50%, and a sharp decrease thereafter. The data reported for the synthetic rubbers [1, 3], however, show a continual decrease in the damping factor with prestrain. Using the definition of equation (2.2-1b), $\alpha=(\omega/c)\tan(\delta/2)$, it is seen that a decrease in the phase velocity would result in an increase in the damping factor; however, the 4% decrease in the phase velocity at 8% prestrain is not sufficient to explain the 15% increase in the damping factor at the same level of prestrain (see Figures 2.4-8 and 2.4-9), therefore it is possible that the loss tangent δ does increase with prestrain for polyethylene.

The work of Lifshitz and Kolsky [44] on the nonlinear viscoelastic creep behavior of polyethylene indicates that this material becomes "stiffer" for additional increments of load as the prestraining is increased for prestrains up to approximately 10%. This is a study of the quasistatic behavior of polyethylene, which provides data in the rubbery region and low end of the transition region on a graph of modulus versus log-frequency. If the "additional increment of load" is interpreted as a dynamic load for which ω is (very) small, then the results of [44] indicate an increase in the "incremental" modulus as the prestrain is increased, which is opposite to the effect indicated at higher frequencies. This means that the two curves given in Figure 2.4-8b must cross as the frequency ω decreases.

The reason for the effects and anomalies discussed above are difficult to assess. Low-density unoriented polyethylene is supposed to be highly amorphous, that is, of low-percent crystallinity, and be non-crosslinked. However, processes for polymerizing ethylene sometimes use catalysts that promote weak cross-linking by side groups (see [58], p. 51). These weak bonds may be ruptured during early stages of strain. The evidence seems to indicate that the phenomenon occurring at low strain is not part of the induced anisotropy resulting from the "orienting and crystallizing" effects of large strains in polymers. It is the latter to which the recent work on nonlinear large-strain theories is primarily directed.

The second major part of this experimental study will now be considered: the propagation of a longitudinal strain pulse in a prestrained polyethylene rod of the same material and geometry as used in the continuous-wave studies. The general experimental problems associated with wave-propagation in viscoelastic materials are discussed in Section 3.1, followed by a summary of the experimental method and details of the experimental apparatus and procedure used in this study.

III. PULSE PROPAGATION EXPERIMENTS

3.1. Introduction

It was found in Part II that high-frequency sinusoidal waves travel at a higher velocity in polyethylene than do low-frequency waves. It was also found that high-frequency waves are attenuated more rapidly than waves of lower frequency. As a result of these two effects the shape of a mechanical pulse changes as it propagates through the viscoelastic material.

It was further found that the phase velocity and attenuation of sinusoidal waves are affected by prestraining the polyethylene material. The analytical and experimental investigation of the influence of prestrain upon the propagation of an incremental longitudinal strain pulse is discussed in the following sections. The analytical method for predicting the speed and shape of the strain pulse is given in Section 3.2. The experimental setup used to induce and measure a strain pulse traveling along a polyethylene rod is described in Section 3.3, and followed by a correlation and discussion of the results.

3.2. The Experimental Method

3.2.1. Theoretical Development

The analytical method used in this study for describing the strain pulse propagating along a slender rod of viscoelastic material with known mechanical properties is essentially the Fourier transform method developed by Hunter [23] for a linear viscoelastic material.

The phenomenon of geometric dispersion is well known; the speed of propagation of a sinusoidal wave along a cylindrical rod of an elastic material depends upon the ratio of the wavelength λ to the radius, a, of the rod. Davies [59] showed, however, that as long as λ/a is greater than about 10 the approximate one-dimensional theory can be used with the elastic wave speed $c = [E/\rho]^{1/2}$. The diameter of the specimen rod used in this study was 1/8 of an inch and the minimum significant wavelength was about 1.4 inches, so that $\lambda/a > 10$. Therefore the approximate one-dimensional theory can be used without introducing any significant error due to geometric dispersion.

The equations necessary for describing a uniaxial wave propagating along a semi-infinite viscoelastic rod are the equation of motion, the strain-displacement equation, the constitutive equation and the initial and boundary conditions. The constitutive equation is here taken in the form of the superposition integral

$$\sigma(t) = E_D \left[\varepsilon(t) - \int_{-\infty}^{t} \phi(t-\tau) \frac{d\varepsilon(\tau)}{d\tau} d\tau \right] \quad . \qquad (3.2\text{-}1)$$

$\phi(t)$ is called the relaxation function for the material, a positive, monotonic function increasing with time and independent of the stress and strain amplitude. The relaxation function and E_D, the dynamic Young's modulus, can be determined by a uniaxial relaxation test. A thin rod of the viscoelastic material is subjected to a step strain, $\varepsilon = \varepsilon_\circ H(t)$, where $H(t)$ is the Heaviside unit function. The resulting stress is given by

$$\begin{aligned} \sigma(t) &= E_D[1-\phi(t)]\varepsilon_\circ \quad , \quad t \geq 0 \\ &= 0 \quad , \quad t<0 \quad . \end{aligned} \qquad (3.2\text{-}2)$$

The equation of motion and strain-displacement equation are given by equations (2.2-2) and (2.2-3), respectively. The initial and boundary conditions for the problem considered here are

$$\varepsilon(x,0) = \frac{\partial\varepsilon(x,0)}{\partial t} = 0, \quad x \geq 0$$

$$\left. \begin{aligned} \varepsilon(0,t) &= h(t) \\ \lim_{x\to\infty} \varepsilon(x,t) &= 0 \end{aligned} \right\} \quad , \quad t>0 \qquad (3.2\text{-}3)$$

It is convenient to transform the complete system of equations (2.2-2, 2.2-3, 3.2-1 and 3.2-3) by the Fourier transform method to obtain the solution to the problem.

The Fourier integral representation of a function f(x,t) may be written [60] as

$$f(x,t) = \frac{1}{\pi}\int_0^\infty \int_0^\infty f(x,t)\cos \omega(t-u)du\, d\omega \qquad (3.2\text{-}4)$$

or equivalently, as the complex transform pair

$$\bar{f}(x,\omega) = \int_0^\infty f(x,t)e^{-i\omega t}dt \quad , \qquad (3.2\text{-}5)$$

$$2\pi f(x,t) = \int_0^\infty \bar{f}(x,\omega)e^{i\omega t}d\omega \quad , \qquad (3.2\text{-}6)$$

where $f(x,t) = 0$ for $t \leq 0$. This represents f(x,t) for all values of $t>0$ if f(x,t) is piecewise differentiable in every finite interval of t, and if the integral

$$\int_{-\infty}^\infty |f(x,t)|\; dt \qquad (2.3\text{-}7)$$

converges uniformly in x. These conditions are satisfied for the field equations in the pulse propagation problem considered here. Applying the definition (3.2-5) to equations (2.2-2) and (2.2-3) gives

$$\frac{\partial\bar{\sigma}}{\partial x} = (i\omega)^2 \rho \bar{u} \quad , \tag{3.2-8}$$

and

$$\bar{\varepsilon} = \frac{\partial\bar{u}}{\partial x} \quad , \tag{3.2-9}$$

respectively. Making use of the convolution theorem in transforming the constitutive equation (3.3-1) gives

$$\bar{\sigma}(x,\omega) = E_D[1+i\omega\bar{\phi}(\omega)]\bar{\varepsilon}(x,\omega) \tag{3.2-10}$$

which may be written as

$$\bar{\sigma}(x,\omega) = E(i\omega)\bar{\varepsilon}(x,\omega) \tag{3.2-11}$$

where the definition of $E(i\omega)$ in terms of the transformed relaxation function follows from equation (3.2-10). $E(i\omega)$, the complex modulus, was introduced in equation (1.2-1); it is a complex function of the real variable ω and relates the amplitude and phase of the periodic stress and strain response. The complex modulus, in the equivalent form of the frequency-dependent phase velocity $c(\omega)$ and damping factor $\alpha(\omega)$, was determined for the polyethylene material in Part II.

The transformed system of equations (3.2-8), (3.2-9) and (3.2-11) may then be combined to give the following equation in terms of the transformed strain $\bar{\varepsilon}$

$$\frac{\partial^2 \bar{\varepsilon}(x,\omega)}{\partial x^2} - \lambda^2 \bar{\varepsilon}(x,\omega) = 0 \qquad (3.2\text{-}12)$$

where the expression for λ^2 is given by equation (2.2-7) and repeated here for convenience

$$\lambda^2 = \frac{(i\omega)^2 \rho}{E^* e^{i\delta}} \quad .$$

The solution to equation (3.2-9) under the conditions (3.2-3) is

$$\bar{\varepsilon}(x,\omega) = \bar{\varepsilon}(0,\omega) e^{-\lambda(i\omega)x} \quad , \qquad (3.2\text{-}13)$$

where $\bar{\varepsilon}(0,\omega)$ is the Fourier transform of the input condition $\varepsilon(0,t)$. The desired time-dependent solution is obtained applying the inverse Fourier transform, defined by (3.2-6) to equation (3.2-13), to give

$$\varepsilon(x,t) = \frac{1}{2\pi} \int_{-\infty}^{\infty} \bar{\varepsilon}(0,\omega) e^{-\alpha(\omega)x} e^{i\omega[t-(x/c(\omega))]} d\omega \quad . \qquad (3.2\text{-}14)$$

Since $\varepsilon(x,t)$ is real, equation (3.2-14) may be written as

$$\varepsilon(x,t) = \frac{1}{\pi}\int_0^\infty [\bar{\varepsilon}_R \cos \omega\{t-(x/c(\omega))\}$$

$$+ \bar{\varepsilon}_I \sin \omega \{ t-(x/c(\omega))\}]\ e^{-\alpha(\omega)x}\ d\omega \qquad (3.2\text{-}15)$$

where $\bar{\varepsilon}(0,\omega)$ has been defined as

$$\bar{\varepsilon}(0,\omega) \equiv \bar{\varepsilon}_R - i\bar{\varepsilon}_I \qquad (3.2\text{-}16)$$

with

$$\bar{\varepsilon}_R = \int_0^\infty \varepsilon(0,t) \cos \omega t\ dt$$

$$\bar{\varepsilon}_I = \int_0^\infty \varepsilon(0,t) \sin \omega t\ dt \quad . \qquad (3.2\text{-}17)$$

If the phase velocity $c(\omega)$ and damping factor $\alpha(\omega)$ are known for a given material and the input boundary condition $\varepsilon(0,t)$ is known for the accessible end of the semi-infinite rod, then equations (3.2-15) and (3.2-17) provide the complete formal description of the wave propagating along the bar. The details of the numerical procedure used to evaluate these equations are given in the following section.

3.2.2. Numerical Integration

The measured strain at the first strain-gage station was used as the input boundary condition $\varepsilon(0,t)$, since use of the input boundary condition at the transmitter bar-polyethylene interface was found not to be feasible for reasons discussed below in Section 3.3.1. The input strain $\varepsilon(0,t)$ was found to be closely approximated by a sequence of connected piecewise-linear segments (see Figure 3.4-14). This permitted the analytical evaluation of $\bar{\varepsilon}_R$ and $\bar{\varepsilon}_I$ in terms of the end points of each time segment and the zero-time intercept and slope of each segment. This greatly reduced the computation time by eliminating the need for the numerical integration of equations (3.2-14) for each value of the circular frequency ω used in numerically evaluating equation (3.2-12).

The resulting expressions for $\bar{\varepsilon}_R$ and $\bar{\varepsilon}_I$ for the piecewise linear approximation to $\varepsilon(0,t)$ are given by

$$\bar{\varepsilon}_R = \sum_{n=1}^{N} (\bar{\varepsilon}_R)_n$$

$$\bar{\varepsilon}_I = \sum_{n=1}^{N} (\bar{\varepsilon}_I)_n \quad , \qquad (3.2\text{-}18)$$

where

$$(\bar{\varepsilon}_R)_n = \frac{S_n}{\omega^2} (\cos \omega t_{n+1} - \cos \omega t_n)$$

$$+ \left(\frac{B_n + S_n \ t_{n+1}}{\omega}\right) \sin \omega t_{n+1} - \left(\frac{B_n + S_n t_n}{\omega}\right) \sin \omega t_n$$

and

$$(\bar{\varepsilon}_I)_n = \frac{S_n}{\omega^2} (\sin \omega t_{n+1} - \sin \omega t_n)$$

$$- \left(\frac{B_n + S_n \ t_{n+1}}{\omega}\right) \cos \omega t_{n+1} + \left(\frac{B_n + S_n t_n}{\omega}\right) \cos \omega t_n \quad . \tag{3.2-19}$$

N is the number of straight-line segments, with the n-th segment having end points t_n and t_{n+1}, slope S_n and a zero-time intercept of B_n. As a check on the error introduced by this approximation, equations (3.2-17) for $\bar{\varepsilon}_R$ and $\bar{\varepsilon}_I$ were evaluated numerically by Newton-Cotes quadrature for a range of circular frequencies ω using values of $\varepsilon(0,t)$ scaled directly from the experimental data. These results were compared with the values for $\bar{\varepsilon}_R$ and $\bar{\varepsilon}_I$ obtained by using equations (3.2-18) and found to differ more than 2% only for values of ω greater than 10^5 per second. As will be shown later, due to the exponential term in the integrand of equation (3.2-15) the contribution to the value of $\varepsilon(x,t)$ for values of ω greater than 10^5 is very small.

The expressions (3.2-18) for $\bar{\varepsilon}_R$ and $\bar{\varepsilon}_I$ were introduced into equation (3.2-15) along with the measured values of the phase velocity $c(\omega)$ and damping factor $\alpha(\omega)$ in the forms given by equations (2.4-1) and (2.4-3), respectively. The resulting integral of equation (3.2-15) was numerically evaluated by a Newton-Cotes quadrature formula of order five (see Ralston [70], pg. 116), which uses a fifth-degree polynomial to fit the integrand function $I(\omega,x,t)$ at six points. The integration was performed over the six-point interval of five panels; the interval was then halved and the integration performed for each half and summed. If the two results differed by more than 0.01 percent the interval was halved and the computations repeated. Panel widths of $\Delta\omega$ = 200 per second were used. The integration was performed over intervals of 1000 per second, starting at $\omega = 0$, and the sum accumulated over successive intervals along the ω-axis.

Two difficulties arose in evaluating equation (3.2-15) numerically: (1) the integrand is indeterminate at $\omega = 0$ in the form in which it appears in equation (3.2-15), i.e., the transforms $\bar{\varepsilon}_R$ and $\bar{\varepsilon}_I$ are fractions whose numerators and denominators vanish at $\omega = 0$, and (2) the upper limit of the integral is not finite. The first problem was solved by applying L'Hospital's Rule in taking the limit of the integrand $I(\omega,x,t)$ as $\omega \to 0$. Using the expressions given by equations (3.2-18) and (3.2-19) for the transform of the piecewise linear approximation to $\varepsilon(0,t)$ and applying L'Hospital's Rule, the limit of the integrand of equation (3.2-15) was found to be finite, say

$$\lim_{\omega \to 0} I(\omega,x,t) = K(x,t) \quad . \tag{3.2-20}$$

It was further found that

$$K(x,t) \cong I(\omega,x,t) \Big|_{\omega=1} \tag{3.2-21}$$

for all values of x and t used in the computations. This result was used for convenience in computing the value of the integrand at $\omega = 0$ in the numerical evaluation of the integral in equation (3.2-15).

The second problem was resolved by determining the magnitude of $\omega = \omega'$ for which

$$\left| \varepsilon(x,t) - \int_0^{\omega'} I(\omega,x,t)d\omega \right| \leq \delta\varepsilon(x,t) \tag{3.2-22}$$

or, equivalently

$$\left| \int_{\omega'}^{\infty} I(\omega,x,t)d\omega \right| \leq \delta \int_0^{\infty} I(\omega,x,t)d\omega \tag{3.2-23}$$

where δ is the relative error. By numerically evaluating the terms in the brackets in the integrand of equation (3.2-15) it was found that the value of the bracketed quantity was positive and approximately equal to 0.086 over the range of circular frequency $0 \leq \omega \leq 10^4$. For $\omega > 10^5$ the magnitude of the bracketed quantity was less than 0.05 and it alternated in sign as ω increased. The following inequality can then be written for the left-hand side of equation (3.2-23)

$$\left| \int_{\omega'}^{\infty} I \, d\omega \right| \leq \int_{\omega'}^{\infty} |I| \, d\omega \leq \int_{\omega'}^{\infty} (0.05) e^{-d\omega x} \, d\omega \tag{3.2-24}$$

for $\omega' \geq 10^5$, with $d = 2.68 \times 10^{-6}$ per second per inch as determined in Part II and $x = 10.4$ for this problem. A lower bound for the integral on the right-hand side of equation (3.2-23) can be written as follows

$$\int_{0}^{10^4} (0.086) \, e^{-d\omega x} \, d\omega \leq \int_{0}^{\infty} I \, d\omega \quad . \tag{3.2-25}$$

The inequality of equation (3.2-23) will then be satisfied if

$$\int_{\omega'}^{\infty} (0.05) \, e^{-dx\omega} \, d\omega \leq \delta \int_{0}^{10^4} (0.086) \, e^{-dx\omega} \, d\omega \quad . \tag{3.2-26}$$

Taking $\delta = 0.001$ in equation (3.2-26) and solving for ω' gives $\omega' \simeq 2.5x10^5$ per second. The Newton-Cotes quadrature formula was then used to sum over up to 250 six-panel intervals of 1000 per second to evaluate the integral of equation (3.2-15) for $\varepsilon(x,t)$. It was found in the process of performing the computations that the sum over the first 150 intervals gave a result for $\varepsilon(x,t)$ that differed by less than 0.1% of the value obtained by integrating over 250 intervals for x=10.4 and several different values of t. To conserve computation time, the value of ω' was taken as $1.5x10^5$ per second in the remainder of the computations.

3.3. Details of the Pulse Propagation Experiment

3.3.1. Experimental Apparatus

The experimental part of the pulse propagation study consisted of inducing a longitudinal tensile strain pulse into a polyethylene rod that was in a state of longitudinal prestrain, and measuring the resulting dynamic strain as a function of time at stations along the rod. The apparatus used to generate and detect the propagating strain pulse is shown schematically in Figure 3.3-10. The system consists of an aluminum transmitter bar, a steel striker bar and the polyethylene rod waveguide. These components were mounted on the lathe bed used previously

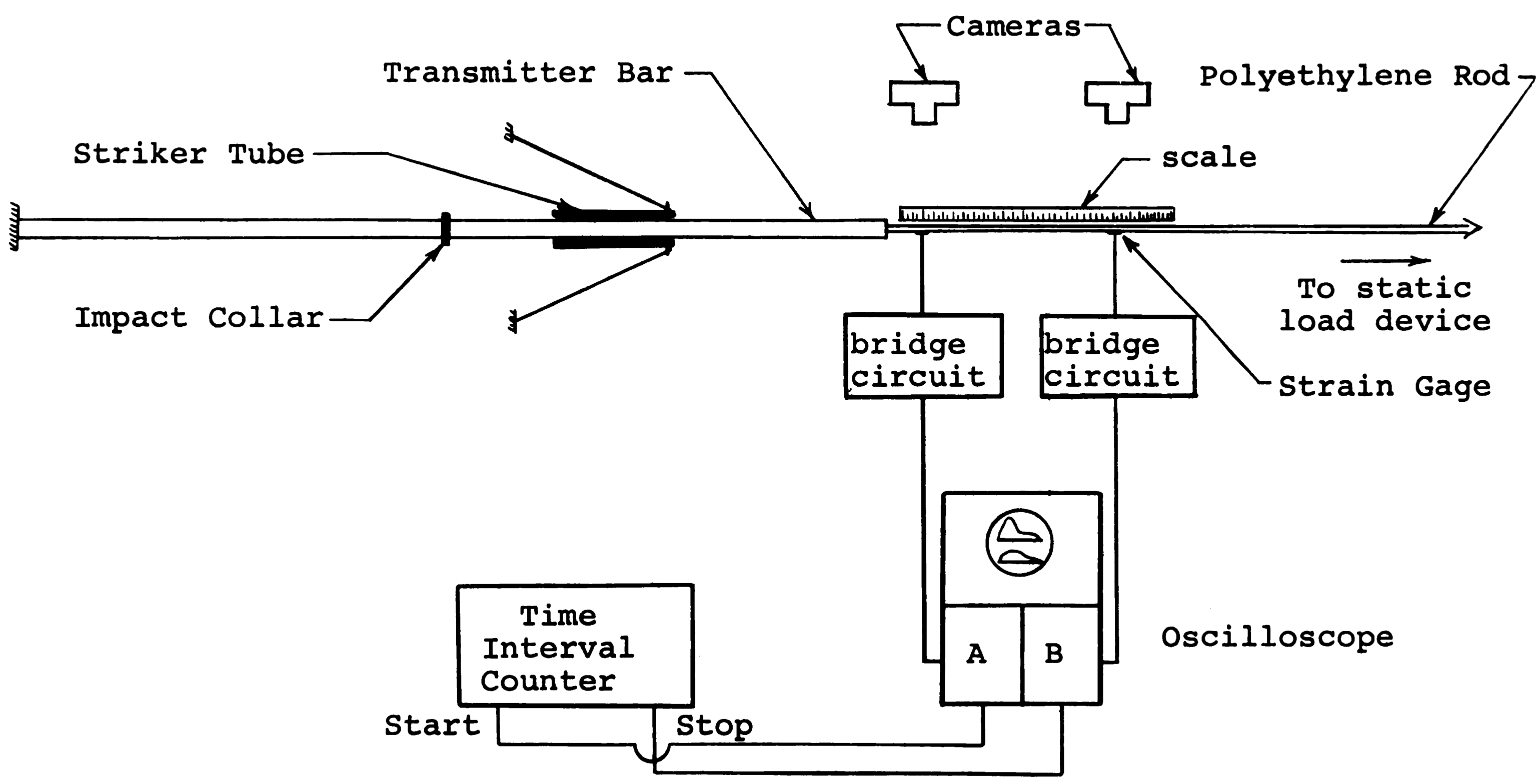

Figure 3.3-10. Schematic Diagram of the Wave-Propagation Experimental Apparatus

(see Section 2.3.2) together with the apparatus to induce the prestrain into the specimen rod. Two strain gages were used to monitor the strain pulse as it propagated along the rod. Details of the strain-gage technique are given in Section 3.3.2 and in Appendix B. Some comments on the strain gage behavior are also included in Section 3.4 in the discussion of the results. The level of static prestrain was recorded photographically as shown schematically in Figure 3.3-10. A photograph of the complete apparatus is shown in Figure 3.3-11.

The specimens used in this study were one-eighth-inch diameter rods of low-density polyethylene, the same as the specimens used to determine the dynamic material properties in the continuous-wave study discussed in Part II. A detailed discussion of the specimens is given in Section 2.3.1.

The device used to generate the strain pulse consists of a 0.375-inch-diameter aluminum rod, 60 inches long, with an impact collar located at the center. The collar is impacted by a sling-shot-propelled concentric striker tube to produce the strain pulse. Figure 3.3-12 shows the details of the transmitter bar-collar-striker tube assembly. At impact a tensile strain pulse travels to the right along the transmitter bar from the impact collar. A similar compressive pulse travels simultaneously to the left. These elastic pulses travel essentially

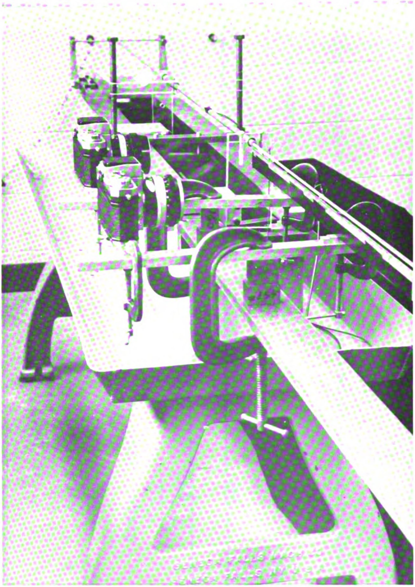

Figure 3.3-11. The Wave-Propagation Experimental Apparatus

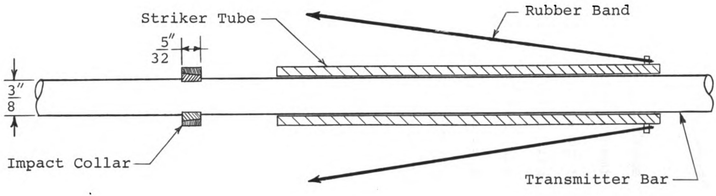

Figure 3.3-12. Details of the Transmitter-Bar-Impact-Collar-Striker Tube Assembly.

undistorted at the sonic velocity of the aluminum. The duration of the pulse is governed by the time required for the pulse to travel twice the length of the striker tube.

The large acoustical-impedence mismatch between the 3/8-inch diameter aluminum transmitter bar and the 1/8-inch diameter polyethylene waveguide results in most of the tensile strain pulse in the aluminum rod being reflected from the aluminum-polyethylene interface as a compressive strain pulse. It can be shown that the stress reflection coefficient for an elastic stress pulse transmitted from rod 1 to rod 2 at an interface is (see Lindsay [61], pg. 74, et.seq.):

$$R = \frac{\rho_2 c_2 A_2 - \rho_1 c_1 A_1}{\rho_2 c_2 A_2 + \rho_1 c_1 A_1} \qquad (3.3\text{-}1)$$

where ρ, c and A are the density, sonic velocity and cross-sectional area of the respective rods at the interface. Assuming for the moment that polyethylene is purely elastic with a sonic velocity c = 30000 inches per second, the resulting reflection is -0.99. Thus, to seek to determine the experimentally transmitted pulse as the difference between the incident and reflected pulse would be to seek the small difference between the incident and reflected pulses, introducing the possibility of large relative errors.

Consequently, the input boundary condition for the strain pulse in the polyethylene rod was taken as the strain measured at the first strain gage, located approximately two inches from the aluminum-polyethylene interface. Figure 3.3-13 shows an oscillogram of the strain as a function of time at both gages. The input pulse duration is approximately 250 microseconds.

The method of attaching the polyethylene rod to the end of the transmitter bar is essentially the same as that used in the continuous-wave study (see Figure 2.3-1). The end of the polyethylene rod was "upset," as described in Section 2.2.2. The resulting bulbous end was then embedded in a 1/4-inch-diameter by 7/16-inch-deep hole in the end of the transmitter bar with a room-temperature-setting epoxy. This provided a connection that would support the static axial load on the polyethylene rod and, at the same time, transmit the propagating pulse from the transmitter bar into the polyethylene rod without apparent distortion. Clamping techniques would have caused the polyethylene to fail by "necking" at the point of clamping, and, in addition, would possibly present a discontinuity in the otherwise "smooth" transmitter bar which would distort the pulse transmitted to the polyethylene specimen.

Prestrain was induced into the polyethylene rod in the same manner as in the continuous wave studies: the far end of the polyethylene rod was passed over a pulley

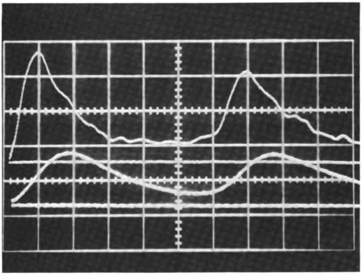

Figure 3.3-13. Typical Oscillogram Record of a Strain Pulse as it Passes the Two Strain-Gage Stations on the Polyethylene Rod. The second pulse on each trace is the reflected pulse from the support-end of the transmitter bar.

and loaded with dead weights. The polyethylene was allowed to creep until the desired level of prestrain was attained, and then the pulley was clamped to maintain the level of prestrain.

3.3.2. Strain Measurement

The strain pulse in the polyethylene rod was measured at two stations with conventional strain gages. Micro-Measurements, Inc., Type EP-08-062AD-120 foil strain gages of 1/16-inch gage length were used. Due to the confining size of the polymer rod only one gage was used at each station. Each strain gage was connected into a four-arm balanced Wheatstone bridge, with a 1.5 volt battery power supply. The bridge output was amplified by a Tektronix Type D High-Gain Differential Calibrated DC Preamplifier and recorded photographically on a Tehtronix Type 555 Dual Beam Oscilloscope. Each channel of the oscilloscope was operated independently, set for single sweep and triggered by the incoming signal from the preamplifier; the vernier trigger adjustment enabled triggering at a very low threshold above the base line. The plus-gate trigger output from the time-base plug-in unit of each channel of the oscilloscope was used to trigger a Computer Measurements Corporation Model 800A/833A time-interval counter. The arrival of the strain pulse at the first gage triggered the sweep of the first oscilloscope trace and "started" the time interval counter; the arrival of the pulse at the second gage triggered the second trace and "stopped" the time interval counter. This resulted in a complete description of the pulse at each gage station and a record of the time of travel of the pulse front from the first gage station to the second. The time-interval counter has a resolution of 0.1 microseconds and an accuracy of ±1 count. A typical oscillogram record of the strain pulse as it is measured at the two strain-gage stations on the polyethylene rod is shown in Figure 3.3-13.

The level of static prestrain and the distance between the strain gages was recorded photographically. A steel scale with 100 divisions per inch was placed parallel and adjacent to the polymer rod; the position of both strain gages relative to the scale was then recorded at the appropriate levels of prestrain. In addition, the static strain level was recorded by d.c.-coupling the strain-gage bridge to the oscilloscope and recording the indicated strain. This permitted a comparison of indicated strain with actual strain to establish an effective gage factor for the strain gages as mounted on polyethylene. This problem is discussed further in Appendix B.

3.3.3. Experimental Procedure

Figure 3.3-10 shows a schematic diagram of the complete experimental apparatus used to generate and measure a tensile strain pulse as it propagates along a polymer rod that is in a state of static prestrain. A photograph of the setup is shown in Figure 3.3-11.

The following specific items of equipment were used in this setup as discussed in detail above:

1. Tektronix Type 555 Dual Beam Oscilloscope.

2. Tektronix Type D High Gain Differential Calibrated DC Preamplifiers.

3. Wheatstone four-arm bridges, 120 ohms per arm, 1.5 volt power supply.

4. Micro-Measurements Type EP-08-125AD-120 (post yield) foil strain gages.

5. Computer Measurements Corporation Model 800A/833A Time Interval Counter.

6. Tektronix Type C-12 Trace-Recording Camera.

The following experimental procedure was used for conducting the pulse-propagation tests:

a. A bulbous end was formed on the polyethylene specimen for attaching it to the transmitter bar. The procedure for accomplishing this is discussed in detail in Section 2.3.2.

b. The strain gages were mounted on the polyethylene rod. This required a special etching procedure to enhance the bond between the gage and the polymer. A complete discussion of this problem is given in Appendix B.

c. The bulbous end of the polymer rod was mounted in the hole in the end of the transmitter bar and banded with a room-temperature-setting epoxy.

d. Strain gage leads were attached directly to the strain gage tabs; no separate soldering terminals were used. Low-temperature (200°F) solder was used, with extreme care exercised at this step so as not to overheat the polyethylene.

e. The electronic equipment was turned on and allowed to warm up and stabilize.

f. The desired level of static prestrain was set by applying a load to the far end, allowing the polyethylene rod to creep until the required prestrain level was attained, and then clamping the pulley to prevent further creeping.

g. The power to the strain-gage bridge was turned on, the "base-line" and strain-gage circuit calibration level were recorded on the oscillogram for each channel.

h. The oscilloscope trace was set to sweep at 50 microseconds per division with a sensitivity of 1 millivolt per division, each channel.

i. The single sweep triggers were reset, the time interval counter register set to zero, and the striker bar manually set and released to induce the strain pulse.

j. The time interval counter read-out was recorded and the oscillogram developed.

k. Steps f through j were repeated for each level of prestrain.

The problem of strain gage failure was experienced for static prestrain levels greater than approximately 5%. Apparent stress concentration in the gage caused the metallic grid of the gage to crack along a line transverse to the axis of the gage and about at the center of the grid pattern. When such a failure occurred the gage was carefully removed and a new gage installed in an adjacent area that had previously been etched. The removal of the broken gage and installation of a new one required approximately 10 minutes. During this time the previously attained level of prestrain was maintained constant. Since it was found in the continuous-wave studies of Part II that the material properties did not change with stress relaxation at a constant level of prestrain, it was assumed here that the time required to install a new gage would not affect the results.

The results of the experimental pulse-propagation tests are given in the following section and compared with the pulse predicted by the analytical method presented in Section 3.2. The results are discussed and compared with the results of other investigators in Section 3.5.

3.4. Numerical and Experimental Results

All of the tests were conducted at an ambient temperature of 72°F ± 1°.

Figures 3.4-14 and 3.4-15 show the experimental and numerical results for the cases of 0.25% prestrain and 8.1% prestrain, respectively. The solid curves give the strain as a function of time as measured experimentally at two gage stations at the given positions on the polyethylene rod. The experimentally-measured strain at the first gage station was then used as the input boundary condition $\varepsilon(0,t)$ to analytically predict the strain as a function of time at the second gage station. The strain pulse at the first strain gage was approximated by a series of connected piecewise-linear segments to decrease computation time, as discussed in Section 3.2.2. These straight-line segments are shown on the record for the first gage in the figures. A tabulation of the appropriate constants for each segment used in the computations with equations (3.2-19) are given in Table 3.4-1. S_n is the slope, B_n is the zero-time intercept and t_n and t_{n+1} are the time-end-points of the n-th segment. Repeatability of the input pulse permitted these tabulated values to be used for the piecewise-linear approximation to the input pulse in both Figure 3.4-14 and Figure 3.4-15.

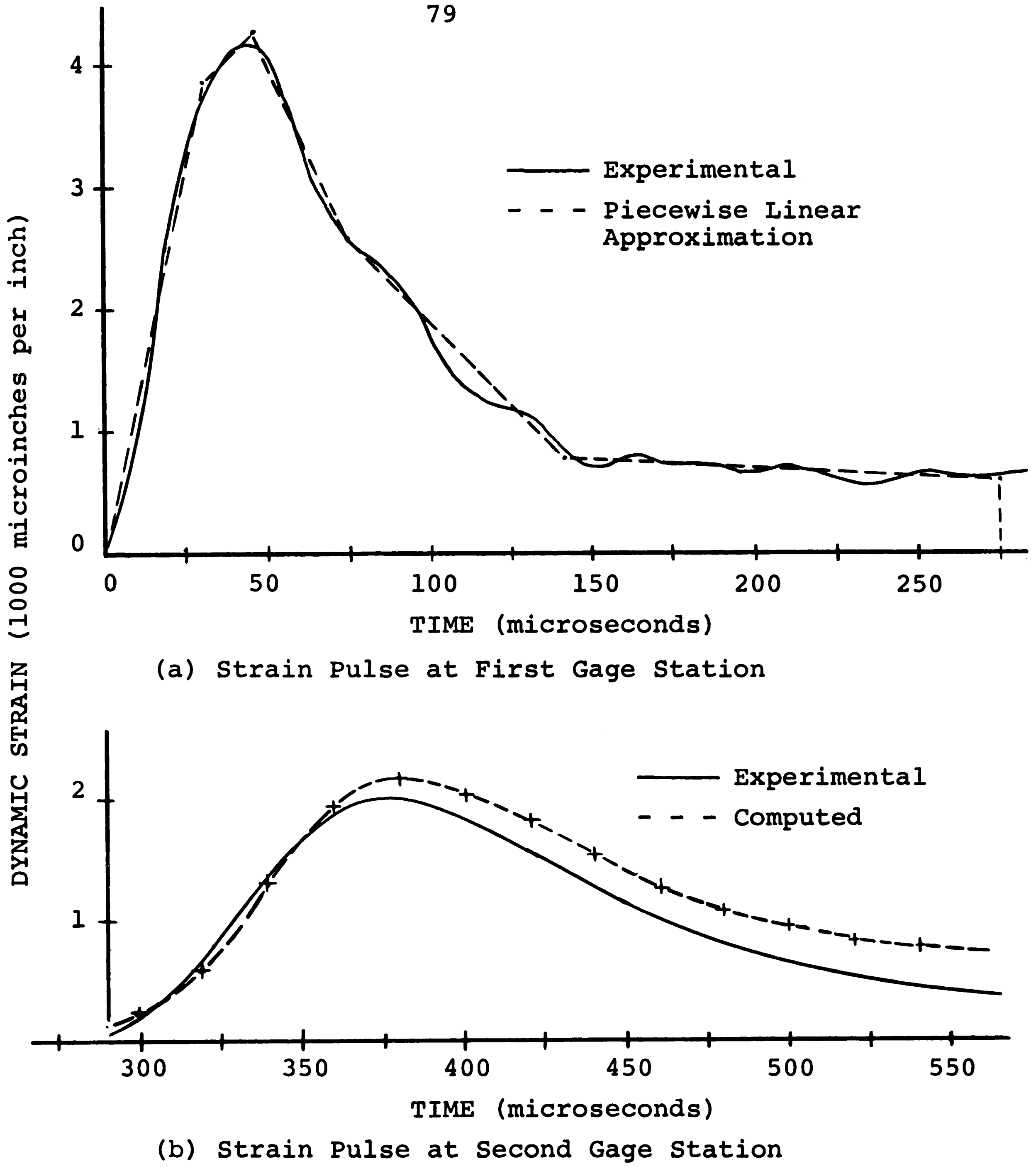

Figure 3.4-14. Numerical and Experimental Results for the Dynamic Strain as a Function of Time at Two Gage Stations 10.42 inches Apart. Prestrain Level of 0.25%; T = 72.5°F.

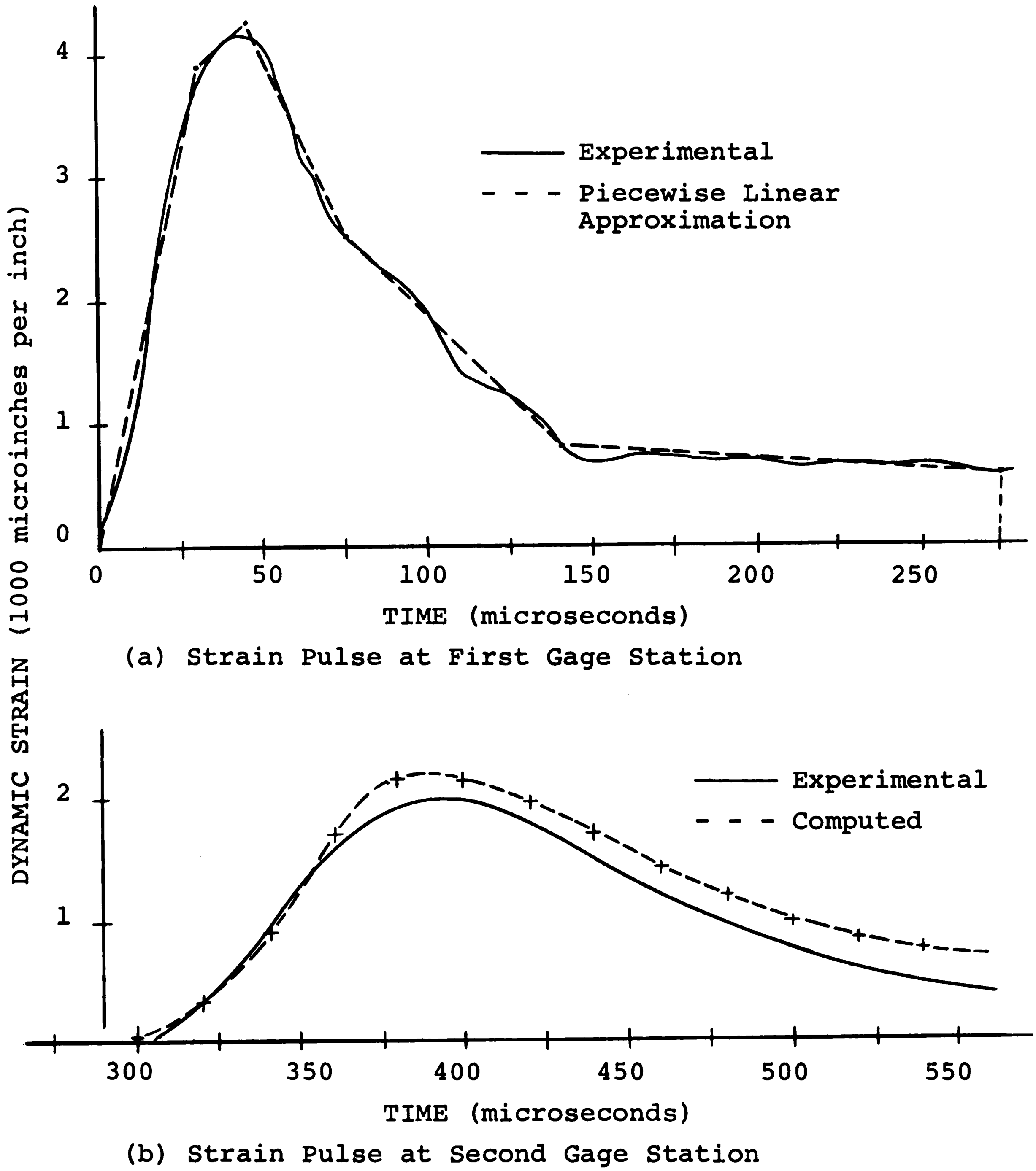

Figure 3.4-15. Numerical and Experimental Results for the Dynamic Strain as a Function of Time at Two Gage Stations 10.39 inches Apart. Prestrain Level of 8.1%; T = 72.5°F.

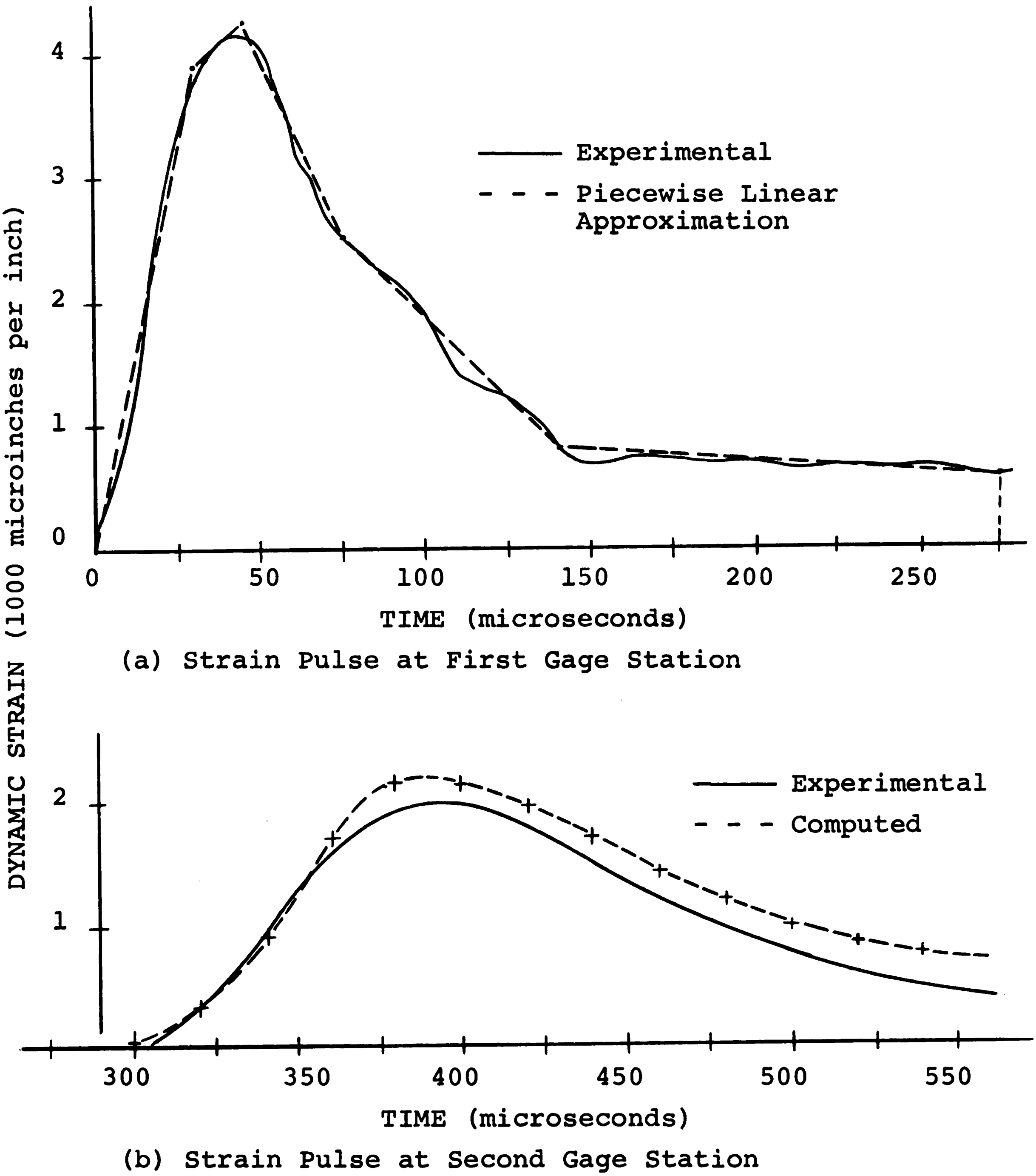

Figure 3.4-15. Numerical and Experimental Results for the Dynamic Strain as a Function of Time at Two Gage Stations 10.39 inches Apart. Pre-strain Level of 8.1%; T = 72.5°F.

TABLE 3.4-1.

THE CONSTANTS FOR EACH SEGMENT OF THE PIECEWISE-LINEAR APPROXIMATION TO THE STRAIN PULSE AT THE FIRST GAGE STATION

Segment	t_n (μ-sec.)	ε_n (μ-in./in.)	B_n (μ-in./in.)	S_n (in./in./sec.)
	0	0		
1			0	128.8
	30	3870		
2			3066	26.7
	45	4270		
3			6856	- 57.8
	75	2530		
4			4532	- 26.7
	140	800		
5			945	- 1.0
	275	670		

t_n, t_{n+1} = time end-points of n-th segment

ε_n, ε_{n+1} = strain at end-points of n-th segment

B_n = zero-time intercept of n-th segment

S_n = slope of n-th segment

The predicted pulse at the second gage station was obtained by numerically integrating equation (3.2-15), using the computed transform of the input boundary condition at the first gage in the form of equations (3.2-18) and the values of the phase velocity $c(\omega)$ and damping factor $\alpha(\omega)$, for the corresponding level of prestrain, determined by the continuous-wave methods in Part II. The predicted pulse is shown by the dashed line for second gage station in Figures 3.4-14 and 3.4-15.

The experimental results were repeatable to within the width of the oscillogram trace. This was determined by using a storage oscilloscope and superposing the traces from several impacts. To insure repeatability it was necessary that the sling-shot propelled striker tube be released at the same distance from the impact collar each time.

The general problem of strain gage application on polyethylene was investigated independently and is discussed in Appendix B. Two effects should be noted here: one, the strain gage, when mounted on a low modulus material such as polyethylene, has a significant stiffening effect in the area of the gage. As a consequence the indicated strain is less than that which would result if the gage were not there. It was possible in this investigation to compare the prestrain in the polyethylene rod as measured by the strain gages with that measured by the photographs of the rod and scale (see Figure 3.3-11). A correction factor of approximately 2.3 was determined; this compared well with similar results of other investigations (see Appendix B) for higher strain rates. It was therefore concluded to assume a rate-independent correction factor, and, equivalently, to use the uncorrected strain pulse measurements directly in the process of Fourier analysis of the pulse from the first strain gage and re-synthesis of the pulse at the second strain-gage position.

The second problem associated with strain gage applications on polymers is that of local heating of the polymer by the gage. The resulting softening of the polymer in the vicinity of the gage may produce erroneous strain indication. This effect is detected by initial drift upon application of power to the strain gage bridge. In this investigation, using a 1.5 volt power supply for the four-arm Wheatstone bridge, the initial drift was approximately equal to the width of the oscillogram trace and therefore considered relatively insignificant.

3.5. Discussion of Results

The results as given graphically in Figures 3.4-14 and 3.4-15 show the correlation between the experimentally-measured pulse and the numerically-synthesized pulse, both for the case of 0.25% prestrain and for 8.1% prestrain.

The wave front correlation is seen to be very good. The high frequency components of the pulse travel the fastest and hence are the first to arrive at the next gage station on the polymer rod. The good wave front correlation supports the value of the phase velocity $c(\omega)$ for high frequency as determined in Part II. For example, in the case of 0.25% prestrain the high-frequency asymptatic value of the phase velocity was taken to be 32,600 inches per second, as suggested by the graph of phase velocity versus frequency, Figure 2.4-8a. This value is supported by the experimental pulse propagation measurements reported in two previous investigations [58, 30] by dividing the distance between monitoring stations by the time of travel of the initial wave front from one station to the next. In both of these investigations [58, 30] the value of $c(\omega)$ for large values of ω was taken as approximately 29,000 inches per second for the polyethylene specimens, and the results showed the experimentally measured wave front to be traveling faster than the numerically-synthesized pulse wave front.

The time required for the pulse front to travel from the first strain gage to the second in the case of 0.25% prestrain was 290 microseconds and for 8.1% prestrain it was 301 microseconds. This increase of 11 microseconds out of 300 microseconds is 3.7% which agrees well with the 4% decrease in phase velocity due to 8.0% prestrain in the continuous-wave study.

The agreement in the general shape of the observed and calculated pulses is also good, but the experimentally-measured values are consistently lower than the predicted values on the decreasing side of the pulse. This could be due to several factors: the phase velocity of the lower-frequency components as determined in Part II could be too low. This would decrease the contribution to the pulse amplitude by those lower frequency components. It is possible that the first gage causes a reflection of some of the incoming pulse resulting in a lower actual pulse being transmitted to the second gage. The existence of such reflection is strongly suggested by the magnitude of the correction factor for stiffening due to the strain gage. Also, the gage correction factor could be frequency dependent. The increasing modulus of the polyethylene with increasing frequency suggests that the strain gage response in following the polymer may be greater for higher frequencies. This would cause the strain gage measurement to be more nearly correct in the area of the wave front, where high frequency components predominate, than in the latter stages of the pulse where the lower frequency components become important. There is also the possibility of errors in the values used for the damping factor at lower frequencies.

IV. SUMMARY AND CONCLUSIONS

The objective of this research was to determine the influence of moderate amounts (up to 10%) of quasi-static prestrain upon the dynamic response of low-density polyethylene when small increments of dynamic strain were superposed on the prestrain. In the distinct absence of a formal theory to describe the exhibited nonlinear behavior, the attitude has been to regard each level of quasistatic prestrain as producing a new material, and to determine the "incremental" material response at each level of prestrain.

The experimental investigation consisted of two major areas: first, sinusoidal continuous-wave propagation studies were made to determine the "incremental" dynamic mechanical properties of low-density unoriented polyethylene, using long 1/8-inch-diameter rod specimens. These properties were determined in the form of the frequency-dependent phase velocity $c(\omega)$ and damping factor $\alpha(\omega)$ for various levels of prestrain up to 10%, and over the frequency range comprising the audio frequency spectrum. Taken together $c(\omega)$ and $\alpha(\omega)$ are equivalent to the complex modulus. In the second study, the propagation of an impact-induced longitudinal tensile strain pulse was investigated, using the same 1/8-inch-diameter polyethylene specimen material as was used in the continuous-wave studies, and at essentially the same levels of prestrain. Although the response of the material to dynamic strains of the order of 10% is nonlinear, the incremental dynamic response for small incremental waves superimposed on prestrains up to 10% was assumed to be linear. The assumption was verified experimentally in the continuous-wave studies. With this assumption the impact-induced pulse propagation problem was then analyzed by Fourier analysis and synthesis using the material properties $c(\omega)$ and $\alpha(\omega)$ determined in the continuous-wave studies.

The experimental results indicate that, for prestrains up to approximately 10%, the phase velocity $c(\omega)$ decreases with increasing prestrain and the damping factor $\alpha(\omega)$ increases with increasing prestrain. For example, an 8% prestrain results in approximately a 4% decrease in the phase velocity and a 15% increase in the damping factor, as shown in Figures 2.4-8 and 2.4-9, respectively. These results show a relatively uniform shift of the phase velocity with prestrain over the audio frequency range. At any particular frequency in this range the shifts in phase velocity and attenuation have a smooth (nearly linear) dependence upon prestrain as indicated in Figure 2.4-7. These results extend the work of previous investigations of the influence of prestrain upon the dynamic mechanical properties of polymers and are in good agreement with those results.

The results of the strain-pulse propagation studies support the conclusions of the continuous-wave studies. The strain pulse propagating along the polymer rod was monitored at two stations. The record of the strain pulse as a function of time at the first station was used as the input boundary condition to predict the pulse at the second station as a function of time, using Fourier transform techniques and the previously-determined material properties. The results show a decrease in the speed of travel of the wave front due to prestrain which is in good agreement with the results of the continuous wave study. The general shape of the measured pulse agrees with the shape of the numerically synthesized pulse; the measured pulse is, however, consistently lower in amplitude over all of the pulse except at the pulse front. This discrepancy is believed to be a result of the stiffening effect of the strain gage when applied to the polyethylene. This problem is discussed further in Appendix B.

Indeed, the question of the applicability of conventional strain gages for polymers of low elastic modulus is a serious one. When a strain gage is mounted on any material a local stiffening is introduced. In the application to metals this stiffening effect is relatively insignificant, but when applied to low-modulus materials the effect is significant. As discussed in Appendix B, a correction factor of approximately 2.3 was required for the strain gage-polyethylene rod configuration used in this study. In further pulse-propagation experiments it would be desirable to use some other sensing device.

Recently [30] a Faraday-principle velocity transducer was used to measure the particle velocity in a polyethylene rod subjected to axial impact. A capacitor transducer has also been used to measure transient pulse shapes in applications where the end of the specimen is accessible. Non-contacting methods of monitoring strains in low modulus materials appear to be advantageous, since the monitoring transducer then does not affect the response of the material. Two such methods would be a diffraction grating technique and an interferometric technique; another would be an optical measuring system which monitors the motion of a line on the specimen.

Uncertainties in the experimental dynamic strain measurements must be reduced before any check of the assumption of a linear "incremental" dynamic material response can be made by pulse-propagation experiments.

It is known, by reports from the vibration field, that many structures containing viscoelastic elements exhibit a nonlinear dynamic response. Both of these circumstances display the need for the development of a nonlinear theory which may be conveniently used in the area of dynamic viscoelasticity.

In conclusion, the work presented here extends the available information on the mechanical properties of low-density polyethylene as a function of frequency and of prestrain. Within the framework of the assumption of the applicability of the linear "incremental" theory of viscoelasticity, these results are supported by two independent studies. Some problems associated with this work have been presented which may motivate further research.

LIST OF REFERENCES

1. Hillier, K. W. and Kolsky, H., "An Investigation of the Dynamic Elastic Properties of Some High Polymers," Proc. Phys. Soc., Vol. 62, 1949, pp. 111-121.

2. Mason, P., "The Influence of Strain Upon the Dynamic Properties of Natural Rubber," Physical Properties of Polymers, Soc. Chem. Industry Monograph #5, London, 1959.

3. Hillier, K. W., "Measurement of the Dynamic Elasticity of Rubber," Inst. of the Rubber Industries, Vol. 26, London, Trans., 1950, pp. 64-77.

4. Weber, W., "Über die Elastizität der Seidenfäden," Pogg. Ann. Physik (2), Vol. 4, 1835, p. 247.

5. Boltzmann, L., Pogg. Ann. Eng., Vol. 7, 1876, p. 624.

6. Gross, B., Mathematical Structures of the Theories of Viscoelasticity, Herrmann et Cie, Paris, 1953.

7. Smith, T. L., "Approximate Equations for Interconverting the Various Mechanical Properties of Linear Viscoelastic Materials," Trans. Soc. Rheol., Vol. II, 1958, pp. 131-151.

8. Marvin, R. S., "A New Approximate Conversion Method for Relating Stress Relaxation and Dynamic Modulus," Physics Review, Vol. 86, 1952, p. 644.

9. Alfrey, T. and Doty, P., "The Methods of Specifying the Properties of Viscoelastic Materials," Jnl. Appl. Phys., Vol. 16, 1945, pp. 700-713.

10. Leaderman, H., Elastic and Creep Properties of Filamentous Materials, The Textile Foundation, Washington, D. C., 1943.

11. Alfrey, Turner, Mechanical Behavior of High Polymers, Interscience Publishers, Inc., New York, 1948.

12. Bland, D. R., The Theory of Linear Viscoelasticity, Pergamon Press, New York, N. Y., 1960.

13. Ferry, J. D., Viscoelastic Properties of Polymers, John Wiley & Sons, Inc., N. Y., 1961.

14. Flügge, W., Viscoelasticity, Blaisdell Publishing Co., Waltham, Mass., 1967.

15. Lee, E. H., "Viscoelastic Stress Analysis," Proc. First Symp. on Naval Structural Mechanics, Pergamon Press, New York, 1960, pp. 456-482.

16. Williams, M. L., "The Structural Analysis of Viscoelastic Materials," AIAA Jnl., Vol. 2, No. 5, 1964, pp. 785-809.

17. Ward, I. M. and Pinnock, P. R., "The Mechanical Properties of Solid Polymers," Brit. J. Appl. Phys., Vol. 17, No. 1, 1966, pp. 3-32.

18. Schapery, R. A., "A Note on Approximate Methods Pertinent to Thermo-viscoelastic Stress Analysis," Graduate Aeronautical Lab., Calif. Inst. of Tech. SM 62-40, Nov. 1962.

19. Schapery, R. A., "Two Simple Approximate Methods of Laplace Transform Inversion for Viscoelastic Stress Analysis," Graduate Aeronautical Lab., Calif. Inst. of Tech. SM 61-23, 1961.

20. Arenz, R. J., "Two-Dimensional Wave Propagation in Realistic Viscoelastic Materials," J. Appl. Mech., Vol. 32, Series E, No. 2, 1965, pp. 303-314.

21. Arenz, R. J., "Uniaxial Wave Propagation in Realistic Viscoelastic Materials," J. Appl. Mech., Vol. 31, Series E, No. 1, 1964, pp. 17-21.

22. Cost, T. L., "Approx. Laplace Transform Inversions in Viscoelastic Stress Analysis," AIAA Jnl., Vol. 12, No. 12, 1964, pp. 2157-2166.

23. Hunter, S. C., "Viscoelastic Waves," Progress in Solid Mechanics, edited by Snedden, I. N. and Hill, R., Vol. 1, North-Holland Pub. Co., Amsterdam, 1960, pp. 3-57.

24. Kolsky, H., "Stress Waves in Solids," Jnl. Sound and Vibration, Vol. 1, 1964, pp. 88-110.

25. Chu, B. T., "Stress Waves in Isotropic Linear Viscoelastic Materials," Jnl. de Mecanique, Vol. 1, 1962, pp. 439-462.

26. Valanis, K. C., "Propagation and Attenuation of Waves in Linear Viscoelastic Solids," Jnl. Math. & Physics, Vol. XLIV, No. 3, 1965, pp. 227-239.

27. Fisher, G. M. C. and Gurtin, M. E., "Wave Propagation in the Linear Theory of Viscoelasticity," Q. Appl. Math., Vol. 23, No. 3, 1965, pp. 257-263.

28. Herrera, I. and Gurtin, M. E., "A Correspondence Principle for Viscoelastic Wave Propagation," Brown University Technical Report No. 25, Feb. 1964.

29. Kolsky, H., "Propagation of Stress Pulses in Viscoelastic Solids," Phil. Mag., Vol. 8, No. 1, pt. 2, 1956, pp. 693-710.

30. Norris, Douglas M., Jr., "Propagation of a Stress Pulse in a Viscoelastic Rod," Exp. Mech., Vol. 7, No. 7, 1967, pp. 297-301.

31. Lifshitz, J. M. and Kolsky, H., "The Propagation of Spherically Divergent Stress Pulses in Linear Viscoelastic Solids," J. Mech. Phys. Solids, Vol. 13, 1965, pp. 361-376.

32. Dally, J. N. and Thau, S. A., "Observations of Stress Wave Propagation in a Half-Place with Boundary Loading," Int. J. Solids Structures, Vol. 3, 1967, pp. 293-308.

33. Daniel, I. M., "Experimental Methods for Dynamic Stress Analysis in Viscoelastic Analysis," Jnl. Appl. Mech., Vol. 32, 1965.

34. Arenz, R. J. and Fourney, M. E., "On the Photoelastic Study of Stress Wave Propagation," Graduate Aeronautical Lab., Calif. Inst. of Tech. SM 61-12, June, 1961.

35. Durelli, A. J., Applied Stress Analysis, Prentice Hall, Inc., Englewood Cliffs, New Jersey, 1967.

36. Green, A. E. and Rivlin, R. S., "The Mechanics of Non-linear Materials with Memory, Part I," Arch. Rat. Mech. Anal., Vol. 1, No. 1, 1957, pp. 1-21.

37. Green, A. E. and Rivlin, R. S. and Spencer, A. J. M., "The Mechanics of Non-linear Materials with Memory, Part II," Arch. Rat. Mech. Anal., Vol. 3, No. 1, 1959, pp. 82-90.

38. Green, A. E. and Rivlin, R. S., "The Mechanics of Non-linear Materials with Memory, Part III," Arch. Rat. Mech. Anal., Vol. 4, No. 5, 1960, pp. 387-404.

39. Lockett, F. J., "Creep and Stress-Relaxation Experiments for Non-linear Materials," Int. J. Engng. Sci., Vol. 3, 1965, pp. 59-75.

40. Ward, I. M. and Onat, E. T., "Nonlinear Mechanical Behavior of Oriented Polypropylene," J. Mech. Phys. Solids, Vol. II, 1963, pp. 217-229.

41. Hadley, D. W. and Ward, I. M., "Non-linear Creep and Recovery Behavior of Polypropylene Fibres," J. Mech. Phys. Solids, Vol. 13, 1965, pp. 397-411.

42. Ward, I. M. and Wolfe, J. M., "The Non-linear Mechanical Behavior of Polypropylene Fibres Under Complex Loading Programs," J. Mech. Phys. Solids, Vol. 14, 1966, pp. 131-140.

43. Onaran, K. and Findley, W. N., "Combined Stress-Creep Experiments on a Nonlinear Viscoelastic Material to Determine the Kernel Functions for a Multiple Integral Representation of Creep," Trans. Soc. Rheol., Vol. 9, 1965, p. 299.

44. Lifshitz, J. M. and Kolsky, H., "Nonlinear Viscoelastic Behavior of Polyethylene," Int. Jnl. of Solids and Structures, Vol. 3, No. 3, 1967, pp. 383-397.

45. Noll, W., "A Mathematical Theory of the Mechanical Behavior of Continuous Media," Arch. Rat. Mech. Anal., Vol. 2, No. 3, 1958, pp. 197-226.

46. Coleman, B. D., and Noll, W., "Foundations of Linear Viscoelasticity," Review of Modern Physics, Vol. 33, 1961, p. 239.

47. Huang, N. C. and Lee, E. H., "Nonlinear Viscoelasticity for Short Time Ranges," J. Appl. Mech., Vol. 33, Series E, No. 2, 1966, pp. 313-321.

48. Lianis, G. and DeHoff, P. H., Jr., "Studies on Constitutive Equations of First and Second Order Viscoelasticity," Purdue Univ., School of Aero., Astro., and Engineering Sciences, Rpt. No. A&ES 64-10, Sept., 1964.

49. Nachunger, R. R. and Calvit, H. H., "On Approximate Constitutive Equations in Nonlinear Viscoelasticity," Univ. of Texas, Engr. Mechanics Res. Lab., Rpt. TR 1019, Aug., 1967.

50. Biot, Maurice A., Mechanics of Incremental Deformation, Wiley & Sons, New York, 1965.

51. Williams, M. L., Landel, R. F. and Ferry, J. D., "The Temperature Dependence of Relaxation Mechanisms in Amorphous Polymers And Other Glass-Forming Liquids," Jnl. Am. Chem. Soc., Vol. 77, 1955, pp. 3701-3707.

52. Hillier, K. W., "The Measurements of Dynamic Elastic Properties," Progress in Solid Mechanics, edited by Sneddon, I. N. and Hill, R., Vol. 2, North-Holland Pub. Co., Amsterdam, 1960, pp. 201-242.

53. Brown, G. W. and Selway, D. R., "Frequency Response of a Photoviscoelastic Material," Exp. Mech., Vol. 4, No. 3, 1964, pp. 57-63.

54. Adkins, Richard L., "Design Considerations and Analysis of a Complex-Modulus Apparatus," Experimental Mechanics, Vol. 6, No. 7, 1966, pp. 362-367.

55. Philbrick, James A., "Determination of the Complex Modulus of Polyethylene," M. S. Thesis, Dept. of Mech. Engr., Univ. of New Hampshire, July, 1965.

56. Ballou, J. W. and Silverman, S., "Young's Modulus of Elasticity of Fibers and Films by Sound Velocity Measurements," Jnl. Acoust. Soc. of Am., Vol. 16, No. 2, 1944, pp. 113-119.

57. Norris, Douglas, M., "Longitudinal Impact of a Thin Viscoelastic Rod," Ph.D. Thesis, Michigan State University, 1962, 69 pp.

58. Tobolsky, A. V., Properties and Structures of Polymers, John Wiley & Sons, N. Y., 1960.

59. Davies, R. M., "A Critical Study of the Hopkinson Pressure Bar," Trans. Royal Soc. London, Series A, Vol. 240, 1948, pp. 375-457.

60. Sneddon, Ian N., Fourier Transforms, McGraw Hill, New York, 1951.

61. Lindsay, Robert B., Mechanical Radiation, McGraw Hill, New York, 1960.

62. Tauchert, T. R., "The Temperature Generated During Torsional Oscillations of Polyethylene Rods," Int. J. Engrg. Sci., Vol. 5, 1967, pp. 353-365.

63. Huang, N. C. and Lee, E. H., "Thermomechanical Coupling Behavior of Viscoelastic Rods Subjected to Cyclic Loading," Jnl. Appl. Mech., Vol. 34E, No. 1, 1967, pp. 127-132.

64. Hunter, S. C., "The Transient Temperature Distribution in a Semi-Infinite Viscoelastic Rod Subject to Longitudinal Oscillations," Int. J. Engrg. Sci., Vol. 5, 1967, pp. 119-143.

65. Perry, R. H., Chilton, C. H. and Kirkpatrick, S. D., Chemical Engineers Handbook, 4th Edition, McGraw-Hill Book Co., Inc., New York, 1950.

APPENDICES

APPENDIX A

THE TEMPERATURE GENERATED DUE TO THE LONGITUDINAL OSCILLATIONS IN THE POLYETHYLENE RODS

When a viscoelastic rod is subjected to a longitudinal oscillating force, part of the mechanical energy supplied by this force is lost to the rod in the form of heat. The mechanical properties of viscoelastic materials are highly temperature sensitive and the heat input to the material by dissipation affects, in turn, the mechanical response of the material. Thus the problem is one of thermomechanical coupling. Several recent papers [62, 63, 64] have treated this problem rigorously, and the reader is referred to these papers for the extensive details of such an analysis.

It is the purpose of this appendix to establish an upper bound for the temperature rise due to mechanical energy dissipation and to show that this temperature rise was small and therefore had an insignificant effect upon the results of the continuous-wave studies discussed in Part II of this work.

To establish the upper bound it is assumed that all of the mechanical energy dissipated in the form of heat is accumulated in the 1/8-inch-diameter polyethylene rod and that no heat is conducted along the rod. Per unit volume of the rod, the total rate of heat accumulating

$\partial Q/\partial t$ is equal to the rate of heat production due to dissipation, assuming that the rate of heat production due to dilatational compression is negligible. The heat equation is then

$$\frac{\partial Q}{\partial t} = c\rho \, \frac{\partial T}{\partial t} = D \quad , \tag{A.1}$$

where the product of the specific heat c and density ρ is called the heat capacity, T is the temperature and D is the dissipation rate.

It is also assumed that all of the mechanical energy lost is transformed into heat energy so that D can be written as

$$D = \sigma \, \frac{\partial \varepsilon}{\partial t} \quad , \tag{A.2}$$

where

$$\sigma = \sigma_o \sin \omega t \quad ,$$

$$\varepsilon = \varepsilon_o \sin (\omega t - \delta) \quad , \tag{A.3}$$

and δ is the usual phase-lag angle. Then, on a per-cycle basis, the energy loss is

$$D' = \int_0^{2\pi/\omega} \sigma \, \frac{d\varepsilon}{dt} \, dt = \pi \sigma_o \varepsilon_o \sin \delta \quad . \tag{A.4}$$

The heat equation (A.1) then gives the temperature rise per cycle to be

$$T' = \frac{1}{c\rho} \pi \sigma_o \varepsilon_o \sin \delta \quad . \tag{A.5}$$

From equation (2.2-10) the displacement at any cross-section along the rod is:

$$u(x,t) = U_o e^{-\alpha x} \sin (\omega t - kx) \quad . \tag{A.6}$$

Since $\alpha << k$, the expression for strain is approximately

$$\varepsilon = \frac{\partial u}{\partial x} \simeq \frac{U_o \omega}{c} e^{-\alpha x} \cos (\omega t - kx) \quad . \tag{A.7}$$

The exponential term serves to concentrate the energy dissipation near the driven end of the rod, especially at higher frequencies. The maximum value of ε_o can then be taken as

$$\varepsilon_o = \frac{U_o \omega}{c} \quad . \tag{A.8}$$

The maximum magnitude of the stress is

$$\sigma_o = E^*(\omega)\ \varepsilon_o \quad . \tag{A.9}$$

The value of the phase angle δ is found, by using equation (2.2-1), to be approximately 8.6 degrees for the polyethylene.

The maximum rate of dissipation occurs at the high frequencies. At $\omega = 10^5$ per second the maximum displacement $U_o = 10$ microinches for which $\varepsilon_o = 33$ microinches per inch. Substituting the approximate values, equation (A.4) gives the dissipation rate per cycle of energy input to the polyethylene rod to be:

$$D' = 3.6 \times 10^{-5} \text{ in-lbf/in}^3\text{/cycle} \quad . \qquad \text{(A.10)}$$

The heat capacity for polyethylene is $c\rho = 180$ in-lbf/in^3/°F [65], and the resulting temperature rise per cycle given by equation (A.5) is

$$T' = \frac{D'}{\rho c} \simeq 2.0 \times 10^{-7} \text{ °F/cycle} \qquad \text{(A.11)}$$

At $\omega = 10^5$ per second the resulting rate of temperature rise is

$$T' \frac{\omega}{2\pi} \simeq 0.003 \text{ °F per second} \qquad \text{(A.12)}$$

Thus, assuming no loss of heat from the polyethylene rod, a temperature rise of 1°F would require 5 minutes.

Since the time required to take a series of measurements in the continuous-wave study of Part II was of the order of 5 minutes it was considered advisable to experimentally measure the temperature rise in the polyethylene rod during a test. A thermocouple made of 0.003 inch diameter copper-constantan wire was used. A Leeds and Northrup Model 8662 potentiometer was used to read the output of the thermocouple. The thermocouple was mounted on the polyethylene rod approximately two inches from the driven end. The thermocouple was glued to the surface of the rod by Eastman 910 Contact Cement.

Tests were conducted by driving the end of the polyethylene at an amplitude equal to or greater than the amplitudes used in the measurements made in the study of Part II. Each test was run until a temperature equilibrium was reached and the resulting change in the potentiometer reading was recorded and converted to a temperature reading. Tests were conducted at five different frequencies over the audio frequency range. The maximum indicated temperature rise was 0.7°F at the highest frequency tested, 10000 cycles per second. The accuracy of the thermocouple was approximately plus or minus 0.5°F, absolute, but somewhat better than this for making relative temperature measurements.

It may be concluded from these results that the temperature rise of the polyethylene rod was small enough that it did not significantly affect the test data.

APPENDIX B

THE BONDING AND CALIBRATION OF STRAIN GAGES ON POLYETHYLENE

Two problems arose in using conventional strain gages to measure the strain in the polyethylene rod in Part III of this work. First, the "wax-like" nature of the surface of the polyethylene made it difficult to effect a reliable bond between the strain gage and the polyethylene. Second, due to the local stiffening effect of the strain gage, the indicated strain was less than the actual strain would have been without the strain gage bonded in place. The methods used in this study to bond strain gages to polyethylene and to calibrate the strain gages for use on polyethylene are discussed below.

The Bonding Problem

The bonding problem was resolved by a method of preparing the surface of the polyethylene to enhance "wetting" of the surface by the adhesive used, Eastman 910 Contact Cement. In the general problem of adhesives, the bond strength is closely related to the degree of attraction of the adhesive to the surface in question, called wetting. The beading of water on a waxed surface is an example of poor wetting. If a drop of liquid adhesive, such as Eastman 910, spreads out quickly over a flat surface, this is an indication of good wetting of the surface by the adhesive. It was found that Eastman 910 Contact Cement and Duco Cement would not adequately wet the surface of untreated polyethylene. Some epoxy cements appeared to wet the polyethylene surface, but all of the bonds failed at a very low level of strain (less than 0.5%). Consequently, as a part of this research program, a method of treating the polyethylene surface was developed to enhance wetting of the polyethylene by the adhesive. Eastman 910 Contact Cement was selected as the adhesive because the adhesive thickness could be made very thin (approximately 0.003 inch) and still maintain good bond strength. A thin adhesive thickness results in less stiffening effect due to the gage.

An etching process was developed for treating the polyethylene surface, using an etchant recommended for preparing Teflon for bonding. The particular etchant used was Tetra-Etch, manufactured by W. L. Gore and Associates, Newark, Delaware. Directions accompanying the etchant were used as a guide in developing the procedure for etching the polyethylene surface. The procedure for preparing the polyethylene surface and installing the strain gages is as follows:

1. If the surface of the polyethylene is rough or uneven, use dry 400 grit silicone carbide sandpaper to lightly sand the surface in the area where the gage is to be applied.

2. Clean the surface of the polyethylene with acetone to remove any oily residue.

3. Apply the etchant liberally to the surface of the polyethylene and allow it to remain on the surface for at least one minute.

4. Wipe the etchant from the surface with a facial tissue. (Kleenex tissues are recommended as being free of dust and powder.)

5. Repeat steps 3 and 4 for a total of at least three applications of the etchant.

6. Using the neutralizer from an Eastman 910 Contact Cement Kit (obtained from Wm. T. Bean, Inc., Detroit, Michigan), apply the neutralizer to the surface of the polyethylene with a cotton-tipped swab and wipe dry with a kleenex. The surface is now ready for cementing the strain gage to it.

7. Cement the strain gage to the polyethylene with Eastman 910 Contact Cement by the standard procedure outlined in the instructions included in the kit.

8. Solder the leads to the strain gage with a low-temperature solder. A 200°F solder is recommended, together with Variac-controlled soldering iron set at a temperature just sufficient to melt the solder. Care should be exercised not to overheat the gage; since the polyethylene is a poor heat sink, temperature build-up is rapid in the gage and may result in damage to the bond.

For the same reason, the current through the gage should be maintained low.

The Calibration Problem

In the procedure in Part III for measuring the strain pulse propagating along the prestrained polyethylene rod, the level of static prestrain was measured by two methods: the actual elongation of the polyethylene rod was measured by recording the longitudinal displacement of two points approximately 10 inches apart on the rod relative to a fixed scale beside the rod (see Figure 3.3-11). The average static strain was then calculated as the change in the distance between the two points, divided by the original distance. At the same time, the corresponding level of static strain indicated by the strain gages was recorded. The average strain was higher than the gage indicated strain by a factor of about 2.4 for strain levels up to approximately 5%. Norris [58] has previously found that, for strain rates in the range of 10^{-4} to 10^{-2} inches per inch per second, the actual strain was higher than the gage indicated strain by a factor of approximately 2.2. Norris mounted foil strain gages on 1/2-inch diameter by 1.5 inch long low-density polyethylene specimen bars and tested them in compression in an Instron Testing Machine. These strain rates are, however, several orders of magnitude lower than the strain rates associated with wave propagation. The above tests are, in effect, comparing the stiffening effect of the mounted gage with the stiffness of the polyethylene in its "rubbery" (very-low frequency) range.

A test was conducted to examine the response of strain gages mounted on low-density polyethylene under conditions of oscillating strain. From Figure 2.4-8a it is seen that at a frequency of 500 cycles per second, or greater, the polyethylene exhibits a stiffness of the order of 2.5 times greater than the quasistatic value. The apparatus for conducting the test is shown schematically in Figure B-16. An aluminum mass was cemented to each end of a low-density polyethylene rod, 1/2 inch in diameter and 6.0 inches in length. This assembly was driven longitudinally at one end by the vibration driver described in Section 2.3.2. The acceleration of each of the aluminum masses was monitored by accelerometers, Endevco Models 2221, with associated charge amplifiers, Endevco Models 2614C, having a system calibration factor of 100 millivolts (peak) per "g" (peak). The acceleration amplitudes of the end-masses were recorded using a Ballantine Model 320 True-Root-Mean-Square Electronic Voltmeter. At the same time, the oscillatory longitudinal strain in the polyethylene rod was monitored by two strain gages (Micro-Measurements, Inc., Type EP-08-125AD-120 foil strain gages with 1/8-inch gage lengths) mounted

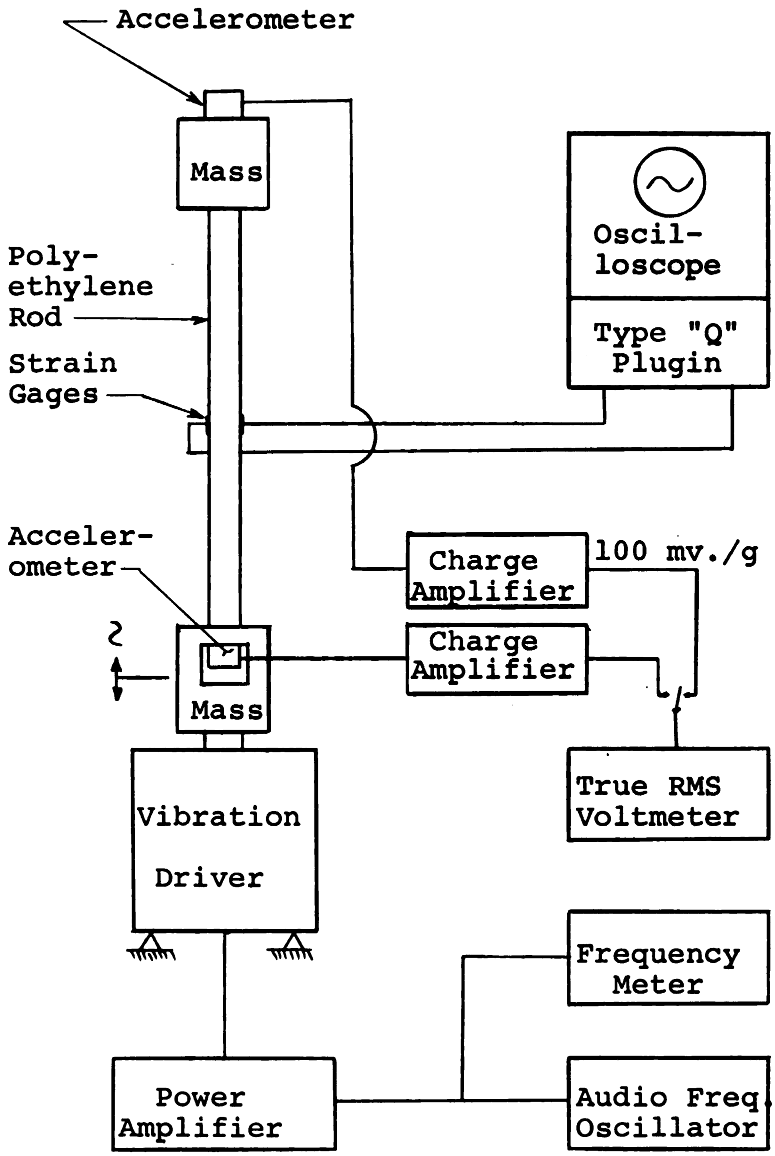

Figure B-16. Schematic Diagram of the Test Apparatus for the Calibration of Strain Gages on a Polyethylene Rod under Sinusoidal Strain.

diametrically opposite and at mid-span on the polyethylene rod. The strain gages were bonded to the rod by the procedure given above in this appendix. The strain gages were connected into a Tektronix Type Q Strain Gage Plug-in Unit mounted in a Tektronix Type 532 oscilloscope. The strain gage system was calibrated by the built-in calibration device in the Q unit. The readings were taken directly from the oscilloscope screen. The strain gage response was then compared to the computed longitudinal strain in the specimen as follows:

The longitudinal resonance of the assembly was found to occur at 452 cycles per second. At this frequency the magnitude of acceleration of the driven-end-mass was 2.83 g's and of the far-end-mass 24.4 g's. Using elementary vibration theory this gives displacement amplitudes of 136 and 1170 microinches, respectively. At resonance the sinusoidal displacements of the two ends are essentially 90 degrees out of phase. When the displacement at the driven end is zero, the displacement at the other end is maximum. This permits the average maximum strain in the rod to be calculated as

$$\varepsilon = \frac{U_L}{L} = \frac{1170\ \mu\ \text{in.}}{6.0\ \text{in.}} = 195\ \mu\text{-in./in.} \tag{B.1}$$

The maximum strain rate for this oscillating strain was $\dot{\varepsilon} = \omega\varepsilon \simeq .5$ inches per inch per second. The strain was assumed to be uniform along the rod since the end mass was large compared to the mass of the polyethylene rod. The corresponding strain indicated by the strain gages was 100 microinches per inch. The computed results are higher than the strain-gage results by a factor of 1.95. This is noted as being lower than the factor of 2.2 for quasistatic strain rates found by Norris [58] on 1/2-inch diameter specimens. This casts some doubt on the assumption, used in Part III, that a single statically-determined correction factor could be applied over the whole frequency range.